

FreeAct: Freeing Activations for LLM Quantization

Xiaohao Liu¹ Xiaobo Xia¹ Manyi Zhang² Ji-Fu Li² Xianzhi Yu²
Fei Shen¹ Xiu Su³ See-Kiong Ng¹ Tat-Seng Chua¹

Abstract

Quantization is pivotal for mitigating the significant memory and computational overhead of Large Language Models (LLMs). While emerging transformation-based methods have successfully enhanced quantization by projecting feature spaces onto smoother manifolds using orthogonal matrices, they typically enforce a rigid *one-to-one* transformation constraint. This static approach fails to account for the dynamic patterns inherent in input activations, particularly within diffusion LLMs (dLLMs) and Multimodal LLMs (MLLMs), where varying token types exhibit distinct distributions. To advance this, we propose FreeAct, a novel quantization framework that relaxes the static one-to-one constraint to accommodate dynamic activation disparities. Theoretically, we leverage the rank-deficient nature of activations to derive a solution space that extends beyond simple inverse matrices, enabling the decoupling of activation transformations from weights. Methodologically, FreeAct identifies token-specific dynamics (*i.e.*, vision *v.s.* text, or masked tokens) and allocates distinct transformation matrices to the activation side, while maintaining a unified, static transformation for the weights. Extensive experiments across dLLMs and MLLMs demonstrate that FreeAct significantly outperforms baselines, up to 5.3% performance improvement, with in-depth analyses. Our code will be publicly released.

1. Introduction

Large Language Models (LLMs) demonstrate remarkable performance across diverse tasks, enabled by pre-training on massive corpora with vast parameter counts (Achiam

¹National University of Singapore ²Huawei Technology
³Central South University. Correspondence to: Xiaobo Xia
<xbx@nus.edu.sg>.

Preprint. March 6, 2026.

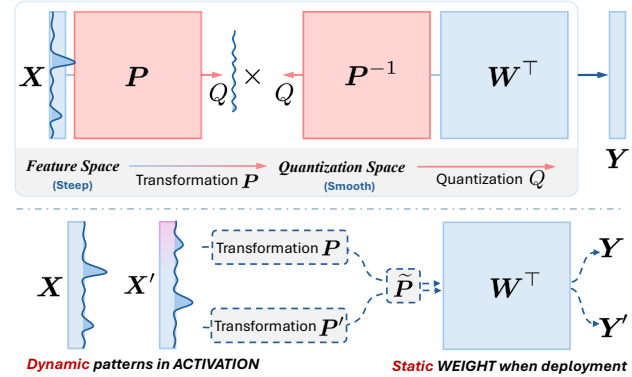


Figure 1. The steep activation is smoothed by the designed transformation matrix for quantization (*top*). One weight corresponds to one transformation to ensure equivalence, *i.e.*, $P \times P^{-1} = I$. In practice, activations are diverse, reflecting dynamic patterns, necessitating flexible transformation matrices on the activation side, while keeping static on the weight side for quantization (*bottom*).

et al., 2023; Touvron et al., 2023; Grattafiori et al., 2024; Yang et al., 2025a; Liu et al., 2024a; Guo et al., 2025b). However, this versatility and generalization come at the cost of significant memory and computation overhead (Kaplan et al., 2020; Zhou et al., 2024; Alizadeh et al., 2024; Liu et al., 2025b; Dai et al., 2025). To maintain capabilities learned from the training stage, yet breaking the efficiency bottlenecks with lower overhead on deployment, recent research pivots toward one critical direction, LLM Quantization (Egashira et al., 2024; Tseng et al., 2024; Xia et al., 2024; Dettmers et al., 2022).

The fundamental goal of *quantization* is to reduce the precision of model parameters and activations (*e.g.*, from BF16 to INT4) (Lin et al., 2025b; Liu et al., 2025c). However, reducing bit-width introduces quantization error, particularly when dealing with significant outliers or non-uniform distribution of values in activations or weights. Conventional methods manage this error by 1) applying clipping thresholds to limit numerical ranges, or 2) employing fine-grained scaling, such as per-token (Zhang et al., 2025b; Xu & Yang, 2025) or per-channel scales (Xiao et al., 2023; Lin et al., 2024b). Recently, transformation-based methods have emerged as a powerful technique (Chee et al., 2023; Tseng et al., 2024; Ashkboos et al., 2024; Lin et al., 2024a; Liu et al., 2024d; Ma et al., 2024), by introducing an orthogonal

matrix P per linear layer to project the steep feature space onto a smoother quantization space, as illustrated at the top of Figure 1. The inverse P^{-1} guarantees the equivalence of computation. One matrix and its unique inverse balance both activation and weight sides within LLMs, *i.e.*, one-to-one transformation. This line of research, exemplified by QuaRot (Ashkboos et al., 2024) and FlatQuant (Sun et al., 2025), offers a new perspective to achieve higher quantization quality¹.

Nevertheless, these methods overlook the dynamic patterns in activations, assuming a consistent behavior that can be handled by the one-to-one transformation. Despite the weights remaining static during inference, input activations can exhibit significant variability, particularly in diffusion LLMs (dLLMs) (Nie et al., 2025; Ye et al., 2025; Wang et al., 2025) or Multimodal LLMs (MLLMs) (Bai et al., 2025; Chen et al., 2024; Guo et al., 2025a), as shown in Figure 2 and Figure 3. The disparities between activations motivate studies on time-aware (dLLMs) (Zhang et al., 2025b; Xu & Yang, 2025) and modality-aware quantization (MLLMs) (Yu et al., 2025). Unfortunately, constrained by the requirement of maintaining a unique inverse matrix to ensure computational equivalence with static weights, they relegate the handling of dynamics solely to the activation-side scaling, neglecting the potential of dynamic transformations.

We pioneer relaxing the static one-to-one transformation constraint in LLM quantization. As illustrated at the bottom of Figure 1, distinct transformation matrices $\{P, P'\}$ are allocated to the activation side to accommodate distinct data types, *e.g.*, vision and text tokens, that exhibit varying dynamic patterns. Meanwhile, the weight side remains static, utilizing a single common transformation \bar{P} . This design frees the activation transformation from the weights, offering new flexibility needed to handle such dynamics and thereby further bolstering quantization quality.

To operationalize this insight, we propose **FreeAct**, a novel post-training quantization method designed to address dynamic activation patterns by breaking the static one-to-one transformation constraint. We first characterize the dynamics arising from diverse token types. Specifically, in dLLMs, we investigate timestep-related variations in activation ranges driven by the significant disparities between masked and unmasked tokens. Similarly, in MLLMs, we observe analogous distinctions between vision and text tokens. FreeAct unifies these paradigms under a common principle. Theoretically, we leverage the rank-deficient nature of activations (Zhang et al., 2024; Jeon et al., 2024) to derive a solution space for transformation relationships that extends beyond simple inverses, confirming the feasibility of FreeAct. Methodologically, we index tokens by type

¹We review the literature related to this work in Appendix B.

and allocate distinct transformation matrices accordingly. For activations, we construct matrices with both shared and unique components, using zero-padding to prevent information entanglement between unique subspaces. Conversely, the weight-side matrix unifies these components while maintaining orthogonality across different subspace bases. We optimize these quantization parameters by minimizing the error *w.r.t.* specific activation types. Furthermore, we provide theoretical guarantees for the equivalence and highlight the implementation simplicity and compatibility with additional enhancements. Extensive experiments on both dLLMs and MLLMs demonstrate that FreeAct achieves superior quantization quality, delivering up to 5.3% relative improvement over state-of-the-art (SOTA) baselines. Further analysis validates the rationale and efficacy of our method. Before delving into details, we summarize our contributions as follows:

- We pioneer relaxing the existing transformation constraint of the activation side to allow for more flexible, dynamic handling of varying activation patterns. Based on this, we unify two advanced LLM paradigms, *i.e.*, dLLMs and MLLMs, under one common principle for quantization.
- We propose FreeAct, a novel post-training quantization framework, utilizing the rank-deficiency of activations to derive distinct transformation matrices for different token types, while maintaining a unified, static transformation for weights. This method effectively handles dynamic patterns through a subspace-based construction and zero-padding strategy with theoretical support.
- We conduct comprehensive experiments across both dLLMs and MLLMs to demonstrate the superior quantization quality of FreeAct and provide in-depth analysis to discuss its rational and effective design.

2. Preliminaries

2.1. Quantization

Setups. Quantization is effective in accelerating the linear inference in networks, especially LLMs.

$$\mathcal{Q}(\mathbf{X}) = \lfloor \mathbf{X}/s_{\mathbf{X}} \rfloor, \quad s_{\mathbf{X}} = \max(|\mathbf{X}|)/q_{\max}. \quad (1)$$

For a linear layer, the computation can be approximated by

$$\mathbf{X}\mathbf{W} \approx \mathcal{Q}(\mathbf{X}) \times \mathcal{Q}(\mathbf{W}) = s_{\mathbf{X}}s_{\mathbf{W}} \cdot \mathcal{Q}_{\mathbf{X}} \times \mathcal{Q}_{\mathbf{W}}. \quad (2)$$

We are focusing on **4-bit** quantization for both weight and activation, *i.e.*, W4A4. Under this setting, the model generally fails to predict reasonable tokens or to follow the instructions (Liu et al., 2025a). The quantization error (Nagel et al., 2021; Li et al., 2024) can be defined as

$$\mathbb{E}(\mathbf{X}, \mathbf{W}) = \|\mathbf{X}\mathbf{W} - \mathcal{Q}(\mathbf{X}) \times \mathcal{Q}(\mathbf{W})\|_F. \quad (3)$$

However, the direct quantization is normally ineffective, especially for cases with *disparities between activations* in Large Language Models (LLMs).

Disparities between activations. The activations exhibit different distributions with different ranges, suggesting that the activations need flexible quantization rather than a fixed process that corresponds to the weight side. In this paper, we explore two representative LLMs: *Diffusion LLMs* (dLLMs) (Nie et al., 2025; Ye et al., 2025) and *Multimodal LLMs* (MLLMs) (Bai et al., 2025; Chen et al., 2024).

- **Mask-aware.** dLLMs predict multiple tokens at newly added [MASK] tokens, which are progressively determined along with the denoising process. From Figure 2, we identify that there are significantly different activation distributions between masked and unmasked tokens.

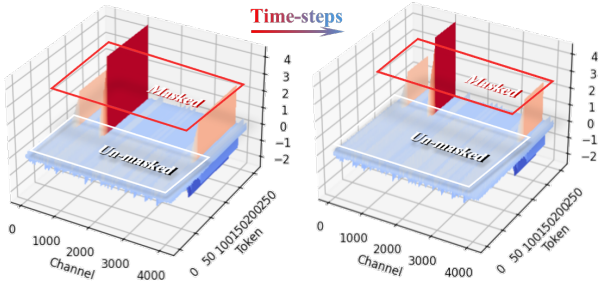


Figure 2. Illustrative example of activations between masked and unmasked tokens along the diffusion time-steps (dLLMs).

- **Modality-aware.** MLLMs process different modalities, e.g., vision and text, as input. Different modality embeddings exhibit different activation distributions, as shown in Figure 3². This disparity, despite being diminished, will be passed to the following layers.

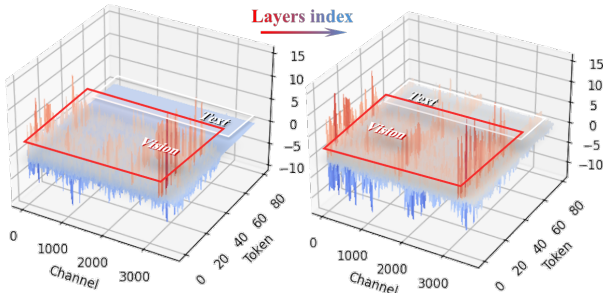


Figure 3. Illustrative example of activation distributions between vision and text tokens at different layers in MLLMs.

From these preliminary investigations, we propose to process these two widely adopted paradigms (Multimodal and diffusion LLMs) under one quantization principle.

²Full visualization will be presented in Appendix D.1 to save the main body space.

2.2. Multimodal and Diffusion LLMs

Learning objective. The learning of dLLMs aims to predict masked tokens with a unified cross-entropy loss (Yang et al., 2025b; Nie et al., 2025):

$$\mathcal{L}_{\mathcal{T}} = -\mathbb{E}_{t, \mathbf{x}_0, \mathbf{x}_t} \left[\frac{1}{t} \sum_l^L \mathbb{I}(\mathbf{x}_t^l = [\text{MASK}]) \log p_{\theta}(\mathbf{x}_0^l | \mathbf{x}_t) \right],$$

where L denotes the sequence length of \mathbf{x}_0 and t is the time step sampled from $[0, 1]$ uniformly, corresponding to \mathbf{x}_t . $\mathbb{I}(\cdot)$ is the indicator. MLLMs predict the next token, while accepting vision and text as input, formally,

$$\mathcal{L}_{\mathcal{M}} = -\mathbb{E}_{\mathbf{x}} \left[\sum_l^L \log p_{\theta}(\mathbf{x}_{l+1} | \mathbf{x}_{<l}) \right]. \quad (4)$$

Here \mathbf{x} is modal-agnostic for simplicity.

Inference. For dLLMs, given one prompt p_0 , the reverse process starts from a fully masked response \mathbf{r}_L . At each intermediate step, tokens with high confidence are confirmed, with the others being remasked for the next step prediction. Specifically, the text sequences are divided into several blocks to mimic an auto-regressive process. For MLLMs, the inference is similar to conventional LLMs, following a next-token prediction manner. Here we handle these two types of models individually, leaving their hybrid version, i.e., Multimodal Diffusion Language Model (Yang et al., 2025b), or other models with heterogeneous token inputs, for future exploration.

3. Methodology

3.1. Beyond One-to-One

One-to-one transformation. Transformation matrices are introduced to model the affine connections among channels. Previous work, like per-channel scaling, can be viewed as a special case, where the matrix is diagonal, i.e., $\mathbf{Y} = \mathbf{X}\mathbf{W} = (\mathbf{X}\text{diag}(\mathbf{c})) \times (\text{diag}(\mathbf{c})^{-1}\mathbf{W}^{\top})$. One matrix for one side, while its inverse is for the other side, to ensure the mathematical equivalence. A more general form can be represented as:

$$\mathbf{Y} = \mathbf{X}\mathbf{P} \times \mathbf{P}^{-1}\mathbf{W}^{\top} \approx \mathcal{Q}(\mathbf{X}\mathbf{P}) \times \mathcal{Q}(\mathbf{P}^{-1}\mathbf{W}^{\top}), \quad (5)$$

where \mathbf{P} is the transformation matrix. FlatQuant (Sun et al., 2025) extends the Hadamard transformation, e.g., QuaRot (Ashkboos et al., 2024), onto the real field \mathbb{R} (i.e., affine transformation) to flatten the steep and dispersed distribution of activations and weights, thus achieving promising results with acceptable computational overhead. This paradigm establishes *one-to-one correspondence* between activations

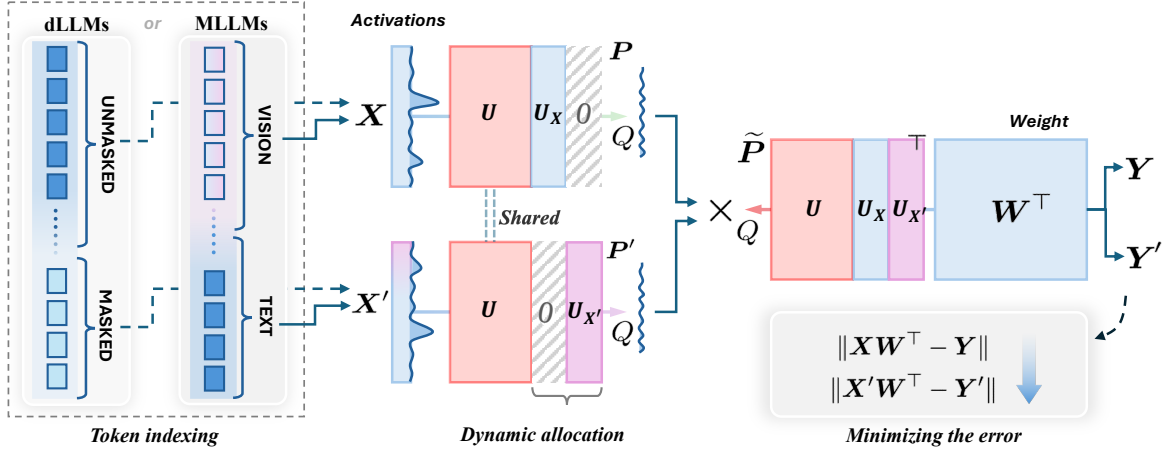


Figure 4. **The overall framework of FreeAct.** Different tokens are indexed to different transformation matrices according to their unique types (vision-text for MLLMs, and unmasked and masked for dLLMs). Different transformation matrices maintain a shared part together while possessing their own uniqueness, where zeros are filled in on another portion. The weight transformation matrix unites both portions to handle all the different activations. And the quantization error is minimized to optimize the quantization parameter.

and weights per layer. P is fixed and shared for the dual side to ensure equivalence, *i.e.*, $PP^{-1} = I$.

Dilemmas. Quantized weights are static during deployment, yet encounter different activation distributions. For instance, the same weights will process activations at different steps and different modal activations in dLLMs and MLLMs, respectively. A *one-fits-all* manner seems limited to handle diverse distributions.

To advance the quantization, we explore new possibilities to free the activation side, especially for models that encounter diverse patterns of activations.

Freeing the activation side. For the static weights, we apply dynamic transformations to match the activations. Formally,

$$\begin{cases} XW^\top = XP \times \tilde{P}W^\top, \\ X'W^\top = X'P' \times \tilde{P}W^\top, \end{cases} \quad \text{s.t. } P \neq P' \quad (6)$$

where P and P' correspond to different activations X and X' . \tilde{P} is determined for weight W . We are resolving these transformations $\{P, P', \tilde{P}\}$ to satisfy the above equations.

We transform this question to resolve an equation with a bilinear constraint, *i.e.*, $XP\tilde{P}W^\top = XW^\top \rightarrow X(P\tilde{P} - I)W^\top = 0$. The trivial solution is to set the middle term $(P\tilde{P} - I)$ as 0, leading to $P = \tilde{P}^{-1}$. Due to the uniqueness of the matrix inverse, for the common transformation of the weight side, there is no choice for the transformation of different activations.

Proposition 1 (Beyond the Inverse). *If satisfy the equation of $XP\tilde{P}W^\top = XW^\top$, the product $P\tilde{P}$ belongs to the set*

$$\left\{ Z - P_X(Z - I)P_W \mid Z \in \mathbb{R}^{d \times d} \right\} \supseteq \{I\}, \quad (7)$$

which strictly contains the singleton $\{I\}$. Consequently, the constraint admits a solution space that is strictly larger than the set of exact inverses (for which $P\tilde{P} = I$).

Remark. $P_X \in \mathbb{R}^{d \times d}$ and $P_W \in \mathbb{R}^{d \times d}$ serve as the orthogonal projections onto the row spaces of activations and weights, satisfying $XP_X = X$ and $P_WW^\top = W^\top$. A special solution is that $P = \tilde{P}$ and $\tilde{P} = \tilde{P}^{-1}$, when $Z = I$. In this case, we assume that the row spaces are of full rank, indicating $P_X = P_W = I$. Therefore, we only consider the singleton $\{I\}$. In general, activations are *rank-deficient* (Zhang et al., 2024), which inspires more solutions to design specific transformations beyond the trivial inverse. Proof is detailed in Appendix A.1.

3.2. FreeAct

To endow activation transformation with more flexibility, we design a new P learning method according to the above proposition by enforcing the low rank at the activation side while ensuring the equivalence. The overall framework is shown in Figure 4. Different tokens are indexed according to different activation transformation matrices, which are implemented via allocation. Weights are also transformed and multiplied by the activations in quantization, followed by the error minimization to optimize quantization parameters.

Token indexing. Given the token sequence x , we first split all tokens into different sets. For the sake of generality, we process two types of tokens once. Therefore, one set of indices can be represented as $\mathcal{I} = \{i \mid \mathbb{I}(x_i = [\text{MASK}]), i \leq L\}$ per sequence, while another is $\mathcal{I}' = \{i \mid \mathbb{I}(x_i \neq [\text{MASK}]), i \leq L\}$. For MLLMs, the indicators are designed to distinguish different modal tokens, *i.e.*,

belonging to vision or text. For each linear layer for quantization, assuming the complete input activations $\hat{\mathbf{X}}$, we have $\mathbf{X} = [\hat{\mathbf{X}}_i]_{i \in \mathcal{I}}$ and $\mathbf{X}' = [\hat{\mathbf{X}}_i]_{i \in \mathcal{I}'}$. These indexed activations will be transformed and then concatenated following the original order for the fidelity of the sequence. Notably, with this formulation, we do not explicitly differentiate the types of LLMs (*i.e.*, MLLMs or dLLMs) in the following.

Dynamic allocation. For different activations $\{\mathbf{X}, \mathbf{X}'\}$, we leverage different transformation matrices, *i.e.*, \mathbf{P} and \mathbf{P}' , to smooth numerical values *w.r.t.* different channels. Specifically, they are constructed with shared and unique components.

$$\begin{aligned} (\mathbf{X}, \mathbf{X}') \begin{cases} \mathbf{P} = [\mathbf{U}, \mathbf{U}_{\mathbf{X}}, \mathbf{0}], & \mathbf{U} \in \mathbb{R}^{d \times r}, \mathbf{U}_{\mathbf{X}} \in \mathbb{R}^{d \times r_1}, \\ \mathbf{P}' = [\mathbf{U}, \mathbf{0}, \mathbf{U}_{\mathbf{X}'}], & \mathbf{U}_{\mathbf{X}'} \in \mathbb{R}^{d \times r_2} \end{cases} \\ (\mathbf{W}) \quad \tilde{\mathbf{P}} = [\mathbf{U}, \mathbf{U}_{\mathbf{X}}, \mathbf{U}_{\mathbf{X}'}]^\top, \quad r + r_1 + r_2 = d \quad (8) \end{aligned}$$

On one hand, \mathbf{U} is designed to preserve the shared row space of the activations, maintained by *all* activations. On the other hand, we manually allocate different activations with different portions, where $\mathbf{U}_{\mathbf{X}}$ and $\mathbf{U}_{\mathbf{X}'}$ are maintained by *distinct* activations. The remaining parts are filled with zeros to avoid any additional information entanglement. This design leads to a well-structured but static weight transformation via $\tilde{\mathbf{P}}$. Once \mathbf{X} is fed into the pre-quantization process, it invokes a low-rank transformation constructed by \mathbf{U} and $\mathbf{U}_{\mathbf{X}}$. Notably, \mathbf{U} , $\mathbf{U}_{\mathbf{X}}$, and $\mathbf{U}_{\mathbf{X}'}$ represent different subspaces bases to avoid any overlap, and the equivalence

$$\mathbf{X}\mathbf{P} \times \tilde{\mathbf{P}}\mathbf{W}^\top = \mathbf{X}\mathbf{W}^\top, \quad \mathbf{X}'\mathbf{P}' \times \tilde{\mathbf{P}}\mathbf{W}^\top = \mathbf{X}'\mathbf{W}^\top \quad (9)$$

can be guaranteed with analyses in Section 3.3. Moreover, we provide in-depth analyses on guarantees and implementations from different perspectives for the crux of FreeAct.

Minimizing the error. We optimize these transformations by minimizing the quantization errors under the structure designed above. Following (Sun et al., 2025), we collect calibration datasets and calculate the differences between the ground truth output and predicted output after quantization. The learning objective is designed per layer:

$$\begin{aligned} \mathcal{L}_q = \mathbb{E}_{x_0} \left[\|\mathbf{X}\mathbf{W} - \mathcal{Q}(\mathbf{X}\mathbf{P})\mathcal{Q}(\tilde{\mathbf{P}}\mathbf{W}^\top)\|_2^2 \right. \\ \left. + \|\mathbf{X}'\mathbf{W} - \mathcal{Q}(\mathbf{X}'\mathbf{P}')\mathcal{Q}(\tilde{\mathbf{P}}\mathbf{W}^\top)\|_2^2 \right]. \quad (10) \end{aligned}$$

We randomly generate orthogonal matrices for initialization, and optimize them *w.r.t.* different activation types. For dLLMs, we distinguish between unmasked and masked tokens, while for MLLMs, we process vision and text tokens individually to avoid the imbalance training.

3.3. Guarantees and Implementations

To further elucidate the theoretical underpinnings and practical deployment of FreeAct, we provide key analyses and implementation details that ground our design choices. Below, we detail the guarantees of equivalence offered by our method, implementation considerations, and additional enhancements that facilitate superior quantization outcomes.

Theorem 2 (Equivalence under projection invariance). *Given $\mathbf{U}, \mathbf{U}_{\mathbf{X}}, \mathbf{U}_{\mathbf{X}'}$ be semi-orthogonal basis matrices forming an orthogonal decomposition of \mathbb{R}^d , such that $\mathbf{X}\mathbf{U}_{\mathbf{X}'} = \mathbf{0}$ and $\mathbf{X}'\mathbf{U}_{\mathbf{X}} = \mathbf{0}$. If we define the orthogonal matrix $\tilde{\mathbf{P}} = [\mathbf{U}, \mathbf{U}_{\mathbf{X}}, \mathbf{U}_{\mathbf{X}'}]^\top$ and the masked transformations \mathbf{P} and \mathbf{P}' , then for any weight matrix \mathbf{W} , the equalities in Eq. (9) hold.*

Remark. This theorem substantiates the theoretical validity of our design based on orthogonal decomposition. It guarantees that the linear operations remain equivalent when distinct activation types are projected onto disjoint basis sets. Proof is detailed in Appendix A.2. In practice, we approach the zero-projection condition (*e.g.*, $\mathbf{X}\mathbf{U}_{\mathbf{X}'} = \mathbf{0}$), rather than enforcing hard constraints, we rely on the minimization of quantization errors to suppress interference between the different token types in Eq. (10).

Core implementation. In practice, FreeAct is simple to implement. Since \mathbf{P} and \mathbf{P}' are built upon the shared orthogonal matrix $\tilde{\mathbf{P}}$, there is no additional memory cost to store \mathbf{P} and \mathbf{P}' . To adapt FreeAct, the first step is to identify different activations. We can directly index the tokens by different `token_id`, like `[MASK]` for diffusion models, and `` for MLLMs. Once $\{r, r_1, r_2\}$ are determined, we can slice $\tilde{\mathbf{P}}$ to yield \mathbf{P} and \mathbf{P}' . We provide the detailed implementation in Appendix C and algorithm flow in Algorithm 1. The slicing procedure can be executed after the transformation. Here we provide the pseudo-code to adapt FreeAct with only three lines of code added before the quantization, as shown below.

```
1 inp = inp @ P # Naive transformation
2 inp[index][..., -r1:] = 0
3 inp[~index][..., -r1-r2:-r1] = 0
```

Additional enhancement. We also adopt more techniques to further enhance the quantization performance. (1) *Learnable Clip Threshold.* This threshold manages the reasonable maximum value of activations or weights, enforcing the smoothness by clipping the values beyond the given threshold. We also free the clip threshold of the activation side to offer more flexibility. (2) *Per-Channel Scale.* This technique operates under the observation of the pattern of different channels, magnifying or shrinking values per channel. The scale for activation and weight

Table 1. Overall performance comparison of FreeAct against quantization methods across four models. The best result in each case is marked in bold, and the averaged value is under the column ‘‘Avg.’’.

	dLLMs				MLLMs			
	HumanEval	GSM8K	Math500	Avg.	MMMU	MMBench	RealworldQA	Avg.
	<i>LLaDA</i>				<i>Qwen2.5-VL</i>			
16-bit Baseline	43.90	76.80	38.40	53.03	50.44	83.25	68.50	67.40
RTN (W8A8)	39.02	77.56	37.00	51.19	49.33	82.38	68.50	66.74
RTN (W4A4)	00.00	00.00	00.14	00.05	26.33	00.09	00.65	09.02
SmoothQuant	00.00	00.00	00.00	00.00	24.41	00.43	01.17	08.67
QuaRot	28.66	65.81	24.20	39.56	43.56	72.51	56.34	57.47
FlatQuant	39.63	74.37	33.60	49.20	48.89	81.61	66.27	65.59
FreeAct (ours)	42.68	75.74	34.60	51.01	50.44	82.22	66.01	66.22
	<i>Dream</i>				<i>InternVL2.5</i>			
16-bit Baseline	56.10	68.16	42.20	55.49	53.22	84.71	68.76	68.90
RTN (W8A8)	48.78	68.76	40.80	52.78	44.33	74.74	63.66	60.91
RTN (W4A4)	00.00	00.53	0.018	00.18	22.78	00.20	00.78	07.92
SmoothQuant	00.00	00.00	0.014	00.05	23.44	00.94	01.05	08.47
QuaRot	39.02	56.56	25.80	40.46	42.19	63.66	54.25	53.36
FlatQuant	46.34	63.53	34.60	48.16	42.11	69.84	57.65	56.53
FreeAct (ours)	50.00	68.84	32.60	50.48	42.44	70.62	58.69	57.25

is entangled to keep the mathematical equivalence, *i.e.*, $Y = (X \cdot \text{diag}(c))(\text{diag}(c)^{-1} \cdot W)$. (3) *Kronecker Product*. To alleviate the computation on matrices P , we adopt two lightweight matrices to construct a larger one, *i.e.*, $P := P_1 \otimes P_r$, following (Chee et al., 2023; Sun et al., 2025). These techniques are compatible with our proposed method, enabling synergies that boost quantization.

Integrations. We integrate FreeAct with both diffusion and multimodal large language models, which adopt the transformation architecture. We employ the matrix transformation for all linear layers in self-attention and feed-forward modules. For the vision tower in MLLMs, we directly implement FlatQuant due to its homogeneous pattern in activations, where only vision tokens are processed. The specific integration of FreeAct for different models, like LLaDA and QwenVL, is detailed in Appendix C.5.

Extensions. FreeAct provides a sound conceptual and practical design for two different activations. However, the philosophy of FreeAct can be extended to 1) more flexible matrix constructions and 2) more modalities. We discuss the possibilities of these two extensions below and leave them for future exploration. (1) Proposition 1 suggests a larger solution space beyond the sole inverse, showing promise to relax the handcraft to a more flexible matrix learned by better optimization objectives. There is a trivial implementation of flex-mode for FreeAct by enlarging the quantization space. In this case, $r_1 = r_2 = d$. It does not assume the explicit shared components *i.e.*, $r = 0$ and $r_1 + r_2 = 2d$, while increasing the memory cost. (2) Moreover, due to the emer-

gence of modalities, like audio (Xu et al., 2025), FreeAct is capable of involving more modalities if more patterns of activations are identified. The trivial extension is adding a new portion $U_{X''} \in \mathbb{R}^{d \times r_3}$ that satisfies $r + r_1 + r_2 + r_3 = d$. In addition, Multimodal Diffusion Large Language Models (MDLLMs) (Yang et al., 2025b) can be viewed as a hybrid problem. To simplify the analysis, in this paper, we do not implement FreeAct with MDLLMs.

4. Experiments

In this section, we conduct experiments to address the following research question:

- **RQ1:** Does our method outperform SOTA quantization methods for dLLMs and MLLMs across diverse benchmarks, to demonstrate its effectiveness?
- **RQ2:** Has the rank-deficiency been verified to support FreeAct? And what is the effect of the additional component that enhances FreeAct?
- **RQ3:** How does FreeAct perform during the training and inference?

4.1. Experimental Setup

Calibration & benchmark datasets. We randomly sample 128 samples with 2048 tokens each from WikiText2 (Merity et al., 2016) to construct the calibration

datasets for dLLMs. We randomly select 256 samples with varying lengths from COCO-Cap (Lin et al., 2014) for MLLMs calibration, including one image and one query each. To evaluate these two LLM types, we select HumanEval (Chen, 2021), GSM8K (Cobbe et al., 2021) (4-shot), and Math500 (Hendrycks et al., 2021) (4-shot) for text tasks on dLLMs. For MLLMs, we select vision-relevant tasks, including MMMU (Yue et al., 2024), MMBench (Liu et al., 2024b), and RealworldQA³. We also report the average value as an overall performance indicator. The dataset descriptions are detailed in Appendix C.1 and C.2.

Base models & baselines. We select two models for each LLM paradigm, including LLaDA (Nie et al., 2025), Dream (Ye et al., 2025), Qwen2.5VL (Bai et al., 2025), and InternVL2.5 (Chen et al., 2024). Built upon these models, we test the quantization quality of FreeAct against RTN, SmoothQuant (Xiao et al., 2023), QuaRot (Ashkboos et al., 2024), and FlatQuant (Sun et al., 2025) under the W4A4 setting. In particular, we also report the results of the 16-bit baseline and RTN in W8A8 for a comprehensive comparison. The details of base models and baselines are shown in Appendix C.3.

Implementation details. With collected calibration datasets, we tune the quantization parameters, including the transformation matrices and clip thresholds, with the AdamW optimizer. The learning rate is set to 1e-3, and the number of training epochs is 15 with a batch size of 4. These settings are kept the same for all the methods. For FreeAct, we set the ratios $r_1 = r_2 = d/k$, and set $k = 32$ by default for simplicity. We also select the front and back layers for FreeAct (see the fully applied version in Section 4.4). We provide more implementation recipes in Appendix C.5.

4.2. Overall Performance (RQ1)

We report the results across different models, datasets, and quantization methods in Table 1. Analyzing the comparative results offers the following three key observations:

① **FreeAct outperforms all quantization baselines, achieving SOTA performance in most scenarios.** Across both dLLM benchmarks (*e.g.*, HumanEval and GSM8K) and MLLM benchmarks (*e.g.*, MMMU and MMBench), FreeAct surpasses existing W4A4 methods in most cases. Notably, it demonstrates superior accuracy retention compared to strong baselines like FlatQuant, achieving up to 5.3% improvement. In several tasks, FreeAct recovers the performance to a level comparable with W8A8 RTN and the 16-bit base models, like in Dream and Qwen2.5VL, highlighting its efficacy in mitigating quantization noise in

³<https://huggingface.co/datasets/xai-org/RealworldQA>.

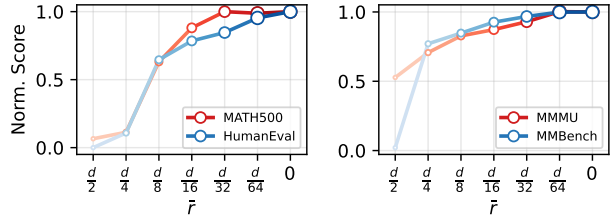


Figure 5. Performance comparison under different rank-deficient settings, tested on LLaDA (left) and Qwen2.5VL (right).

ultra-low bit-width settings.

② **The transformation method is better than simple channel-wise quantization (SmoothQuant).** The results indicate a clear performance gap between transformation-based methods (FreeAct, FlatQuant, QuaRot) and simple scaling methods like SmoothQuant. While SmoothQuant mitigates outliers via channel-wise scaling, it struggles to fully suppress quantization errors in the presence of complex activation patterns under the low-bit scenario. FreeAct, by employing a more sophisticated transformation strategy, effectively flattens the activation distribution, making it more amenable to W4A4 quantization.

③ **The larger flexibility on the transformation matrices provides the possibility to achieve better quantization quality.** Comparing FreeAct against FlatQuant and QuaRot reveals that increased flexibility within the transformation matrix is crucial. FlatQuant eases the Hadamard transformations in QuaRot and employs an affine flexibility, yet it remains tethered to a one-to-one mapping. FreeAct evolves this by breaking this constraint, allowing for a many-to-one transformation. This increased flexibility allows FreeAct to better accommodate diverse activation distributions, resulting in superior quantization quality.

4.3. Ablation Study (RQ2)

Rank-deficient verification. We further investigate the necessity of full-rank transformations by implementing low-rank one-to-one transformation variants. Comparisons on two different models are reported in Figure 5, where \bar{r} denotes the number of removed dimensions, and 0 represents the full-rank transformation. We can observe that a large portion of the removal is incapable, while removing $d/32$ or $d/64$ can approach the upper bound performance. These results confirm our motivation for the rank-deficiency and the feasibility of developing FreeAct.

The effect of learnable clip threshold. We isolate the contribution of the transformation matrix from clipping threshold tuning to evaluate a “clean” version of FreeAct (w/o L.C.) where only the transformation matrix is learned. The results indicate that the optimized transformation matrix is the primary driver of FreeAct’s success in most cases, like

Table 2. Performance comparison with FreeAct without a learnable clip threshold (L.C.).

	LLaDA		Dream	
	Math	HumanEval	Math	HumanEval
FreeAct _{w/o} L.C.	73.09	34.15	55.65	34.14
FreeAct	75.74	34.60	68.84	50.00

	Qwen2.5VL		InternVL2.5	
	MMMU	MMBench	MMMU	MMBench
FreeAct _{w/o} L.C.	46.44	79.30	40.22	65.12
FreeAct	50.44	82.22	42.44	70.62

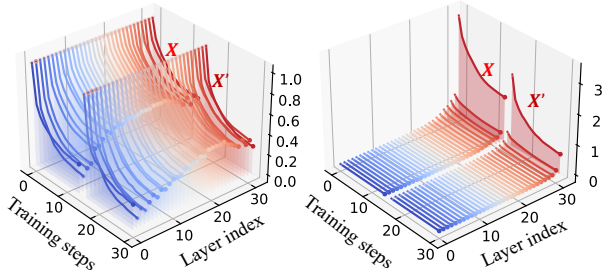


Figure 6. Quantization errors optimized along with the training steps across different layers. X and X' denote different activation types, *i.e.*, masked and unmasked token. The values in the left figure are normalized per layer.

LLaDA. The clip threshold also contributes to capturing the dynamics, especially in Dream, where performance drops with a noticeable margin, suggesting a synergy produced by both the transformation and clip threshold.

4.4. Further Analysis (RQ3)

The loss of quantization errors. We analyze the training dynamics of FreeAct by plotting the quantization error over time as shown in Figure 6⁴. We observe a consistent decrease in Mean Squared Error (MSE) for both types of activations. We also observe the different quantization error ranges between different types ($X > X'$), which suggests the need for a dynamic process. The convergence behavior confirms that FreeAct effectively optimizes the quantization parameters during the calibration phase, progressively minimizing the information loss caused by low-bit quantization.

Activation visualization after transformation. We illustrate the smoothed activation ranges after applying the FreeAct transformation in Figure 7. Compared to the original activations. Applying the transformation successfully redistributes the activation values into a narrower, more uniform range. This smoothing effect ensures that the limited bins available in W4A4 quantization are utilized more efficiently, directly correlating with the reduced quantization error observed in our quantitative analysis.

Applying all layers with the fixed ratio. FreeAct provides more flexibility on the transformation matrix for each layer.

⁴The complete curves for four models are in Appendix D.1.

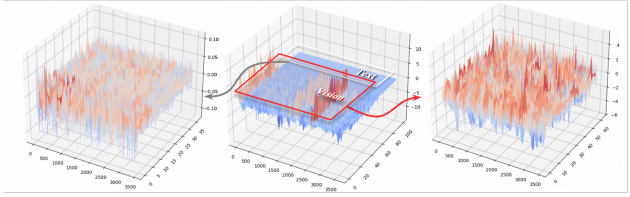


Figure 7. Activation distributions after the transformation.

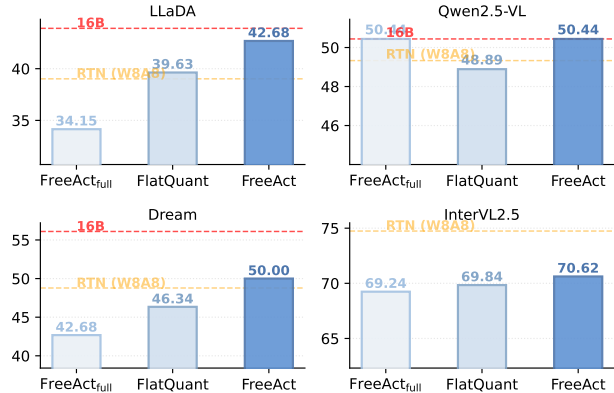


Figure 8. Performance comparison across FlatQuant and fully applied FreeAct.

However, the fixed mask ratio for all layers is not optimal. We show the comparison results with this fully applied version, FreeAct_{full}, as shown in Figure 8. Simply enforcing the activation isolation in FreeAct to every layer would lead to a worse performance in some cases, like on LLaDA or Dream, or perform well on Qwen2.5VL. This suggests the promise of FreeAct, where sophisticated strategies would further boost FreeAct.

5. Discussions and Outlook

In this paper, we introduced FreeAct, a novel post-training quantization framework that breaks the conventional one-to-one transformation constraint prevalent in current LLM quantization methods. By identifying the limitations of static transformations in handling the dynamic activation patterns of advanced models, like dLLMs and MLLMs, we proposed a paradigm shift towards flexible activation transformations. Theoretical analysis of the rank-deficient nature of activations allowed us to decouple the activation transformation from the weight transformation. FreeAct successfully allocates distinct transformation matrices to different token types while maintaining a unified, static transformation for weights. Our extensive experiments demonstrate that FreeAct effectively mitigates quantization errors arising from dynamic disparities. FreeAct establishes a robust foundation for dynamic transformation in quantization, paving several promising avenues for future explorations: 1) extending this framework to more modalities or hybrid model architectures, 2) investigating hardware-kernel co-design for full exploitation, and 3) generalizing to automatically token identification rather than indexing on predefined types.

References

- Achiam, J., Adler, S., Agarwal, S., Ahmad, L., Akkaya, I., Aleman, F. L., Almeida, D., Altenschmidt, J., Altman, S., Anadkat, S., et al. Gpt-4 technical report. *arXiv preprint arXiv:2303.08774*, 2023.
- Alizadeh, K., Mirzadeh, S. I., Belenko, D., Khatamifard, S., Cho, M., Del Mundo, C. C., Rastegari, M., and Farajtabar, M. Llm in a flash: Efficient large language model inference with limited memory. In *ACL*, pp. 12562–12584, 2024.
- Ashkboos, S., Mohtashami, A., Croci, M. L., Li, B., Cameron, P., Jaggi, M., Alistarh, D., Hoefler, T., and Hensman, J. Quarot: Outlier-free 4-bit inference in rotated llms. In *NeurIPS*, pp. 100213–100240, 2024.
- Bai, S., Chen, K., Liu, X., Wang, J., Ge, W., Song, S., Dang, K., Wang, P., Wang, S., Tang, J., et al. Qwen2. 5-vl technical report. *arXiv preprint arXiv:2502.13923*, 2025.
- Bhalgat, Y., Lee, J., Nagel, M., Blankevoort, T., and Kwak, N. Lsq+: Improving low-bit quantization through learnable offsets and better initialization. In *CVPR*, pp. 696–697, 2020.
- Bondarenko, Y., Del Chiaro, R., and Nagel, M. Low-rank quantization-aware training for llms. *arXiv preprint arXiv:2406.06385*, 2024.
- Chang, Y., Wang, X., Wang, J., Wu, Y., Yang, L., Zhu, K., Chen, H., Yi, X., Wang, C., Wang, Y., et al. A survey on evaluation of large language models. *ACM Transactions on Intelligent Systems and Technology*, 15(3):1–45, 2024.
- Chee, J., Cai, Y., Kuleshov, V., and De Sa, C. M. Quip: 2-bit quantization of large language models with guarantees. In *NeurIPS*, pp. 4396–4429, 2023.
- Chen, M. Evaluating large language models trained on code. *arXiv preprint arXiv:2107.03374*, 2021.
- Chen, M., Shao, W., Xu, P., Wang, J., Gao, P., Zhang, K., and Luo, P. Efficientqat: Efficient quantization-aware training for large language models. In *ACL*, pp. 10081–10100, 2025.
- Chen, Z., Wu, J., Wang, W., Su, W., Chen, G., Xing, S., Zhong, M., Zhang, Q., Zhu, X., Lu, L., et al. Internvl: Scaling up vision foundation models and aligning for generic visual-linguistic tasks. In *CVPR*, pp. 24185–24198, 2024.
- Cobbe, K., Kosaraju, V., Bavarian, M., Chen, M., Jun, H., Kaiser, L., Plappert, M., Tworek, J., Hilton, J., Nakano, R., et al. Training verifiers to solve math word problems. *arXiv preprint arXiv:2110.14168*, 2021.
- Dai, G., Hong, K., Mao, Q., Li, X., Xu, J., Huang, H., Xia, H., Ning, X., Yan, S., Liang, Y., et al. Flashdecoding++next: High throughput llm inference with latency and memory optimization. *IEEE Transactions on Computers*, 2025.
- Dettmers, T., Lewis, M., Belkada, Y., and Zettlemoyer, L. Gpt3. int8 (): 8-bit matrix multiplication for transformers at scale. In *NeurIPS*, pp. 30318–30332, 2022.
- Du, D., Zhang, Y., Cao, S., Guo, J., Cao, T., Chu, X., and Xu, N. Bitdistiller: Unleashing the potential of sub-4-bit llms via self-distillation. *arXiv preprint arXiv:2402.10631*, 2024.
- Egashira, K., Vero, M., Staab, R., He, J., and Vechev, M. Exploiting llm quantization. In *NeurIPS*, pp. 41709–41732, 2024.
- Frantar, E., Ashkboos, S., Hoefler, T., and Alistarh, D. Gptq: Accurate post-training quantization for generative pre-trained transformers. *arXiv preprint arXiv:2210.17323*, 2022.
- Grattafiori, A., Dubey, A., Jauhri, A., Pandey, A., Kadian, A., Al-Dahle, A., Letman, A., Mathur, A., Schelten, A., Vaughan, A., et al. The llama 3 herd of models. *arXiv preprint arXiv:2407.21783*, 2024.
- Guo, D., Wu, F., Zhu, F., Leng, F., Shi, G., Chen, H., Fan, H., Wang, J., Jiang, J., Wang, J., et al. Seed1. 5-vl technical report. *arXiv preprint arXiv:2505.07062*, 2025a.
- Guo, D., Yang, D., Zhang, H., Song, J., Zhang, R., Xu, R., Zhu, Q., Ma, S., Wang, P., Bi, X., et al. Deepseek-r1: Incentivizing reasoning capability in llms via reinforcement learning. *arXiv preprint arXiv:2501.12948*, 2025b.
- Hendrycks, D., Burns, C., Kadavath, S., Arora, A., Basart, S., Tang, E., Song, D., and Steinhardt, J. Measuring mathematical problem solving with the math dataset. *arXiv preprint arXiv:2103.03874*, 2021.
- Hu, X., Cheng, Y., Yang, D., Xu, Z., Yuan, Z., Yu, J., Xu, C., Jiang, Z., and Zhou, S. Ostquant: Refining large language model quantization with orthogonal and scaling transformations for better distribution fitting. *arXiv preprint arXiv:2501.13987*, 2025.
- Jeon, H., Kim, Y., and Kim, J. L4q: Parameter efficient quantization-aware fine-tuning on large language models. arxiv 2024. *arXiv preprint arXiv:2402.04902*, 2024.
- Jin, Z., Wang, B., Lin, X., Bing, L., and Sun, A. On the role of discreteness in diffusion llms. *arXiv preprint arXiv:2512.22630*, 2025.

- Kaddour, J., Harris, J., Mozes, M., Bradley, H., Raileanu, R., and McHardy, R. Challenges and applications of large language models. *arXiv preprint arXiv:2307.10169*, 2023.
- Kaplan, J., McCandlish, S., Henighan, T., Brown, T. B., Chess, B., Child, R., Gray, S., Radford, A., Wu, J., and Amodei, D. Scaling laws for neural language models. *arXiv preprint arXiv:2001.08361*, 2020.
- Li, M., Lin, Y., Zhang, Z., Cai, T., Li, X., Guo, J., Xie, E., Meng, C., Zhu, J.-Y., and Han, S. Svdquant: Absorbing outliers by low-rank components for 4-bit diffusion models. In *NeurIPS*, 2024.
- Lin, H., Xu, H., Wu, Y., Cui, J., Zhang, Y., Mou, L., Song, L., Sun, Z., and Wei, Y. Duquant: Distributing outliers via dual transformation makes stronger quantized llms. In *NeurIPS*, pp. 87766–87800, 2024a.
- Lin, H., Xu, H., Wu, Y., Guo, Z., Zhang, R., Lu, Z., Wei, Y., Zhang, Q., and Sun, Z. Quantization meets dllms: A systematic study of post-training quantization for diffusion llms. *arXiv preprint arXiv:2508.14896*, 2025a.
- Lin, J., Tang, J., Tang, H., Yang, S., Chen, W.-M., Wang, W.-C., Xiao, G., Dang, X., Gan, C., and Han, S. Awq: Activation-aware weight quantization for on-device llm compression and acceleration. In *MLSys*, pp. 87–100, 2024b.
- Lin, T.-Y., Maire, M., Belongie, S., Hays, J., Perona, P., Ramanan, D., Dollár, P., and Zitnick, C. L. Microsoft coco: Common objects in context. In *ECCV*, pp. 740–755, 2014.
- Lin, Y., Tang, H., Yang, S., Zhang, Z., Xiao, G., Gan, C., and Han, S. Qserve: W4a8kv4 quantization and system co-design for efficient llm serving. In *MLSys*, 2025b.
- Liu, A., Feng, B., Xue, B., Wang, B., Wu, B., Lu, C., Zhao, C., Deng, C., Zhang, C., Ruan, C., et al. Deepseek-v3 technical report. *arXiv preprint arXiv:2412.19437*, 2024a.
- Liu, R., Sun, Y., Zhang, M., Bai, H., Yu, X., Yu, T., Yuan, C., and Hou, L. Quantization hurts reasoning? an empirical study on quantized reasoning models. *arXiv preprint arXiv:2504.04823*, 2025a.
- Liu, X., Xia, X., Zhao, W., Zhang, M., Yu, X., Su, X., Yang, S., Ng, S.-K., and Chua, T.-S. L-mtp: Leap multi-token prediction beyond adjacent context for large language models. *NeurIPS*, 2025b.
- Liu, Y., Duan, H., Zhang, Y., Li, B., Zhang, S., Zhao, W., Yuan, Y., Wang, J., He, C., Liu, Z., et al. Mmbench: Is your multi-modal model an all-around player? In *ECCV*, pp. 216–233, 2024b.
- Liu, Z., Oguz, B., Zhao, C., Chang, E., Stock, P., Mehdad, Y., Shi, Y., Krishnamoorthi, R., and Chandra, V. Llm-qat: Data-free quantization aware training for large language models. In *ACL Findings*, pp. 467–484, 2024c.
- Liu, Z., Zhao, C., Fedorov, I., Soran, B., Choudhary, D., Krishnamoorthi, R., Chandra, V., Tian, Y., and Blankevoort, T. Spinquant: Llm quantization with learned rotations. In *ICLR*, 2024d.
- Liu, Z., Zhao, C., Huang, H., Chen, S., Zhang, J., Zhao, J., Roy, S., Jin, L., Xiong, Y., Shi, Y., et al. Paretoq: Scaling laws in extremely low-bit llm quantization. *arXiv preprint arXiv:2502.02631*, 2025c.
- Loshchilov, I. and Hutter, F. Decoupled weight decay regularization. *arXiv preprint arXiv:1711.05101*, 2017.
- Luo, R., Xia, X., Wang, L., Chen, L., Shan, R., Luo, J., Yang, M., and Chua, T.-S. Next-omni: Towards any-to-any omnimodal foundation models with discrete flow matching. *arXiv preprint arXiv:2510.13721*, 2025.
- Lyu, C., Wu, M., Wang, L., Huang, X., Liu, B., Du, Z., Shi, S., and Tu, Z. Macaw-llm: Multi-modal language modeling with image, audio, video, and text integration. *arXiv preprint arXiv:2306.09093*, 2023.
- Ma, Y., Li, H., Zheng, X., Ling, F., Xiao, X., Wang, R., Wen, S., Chao, F., and Ji, R. Affinequant: Affine transformation quantization for large language models. *arXiv preprint arXiv:2403.12544*, 2024.
- Merity, S., Xiong, C., Bradbury, J., and Socher, R. Pointer sentinel mixture models. *arXiv preprint arXiv:1609.07843*, 2016.
- Nagel, M., Fournarakis, M., Amjad, R. A., Bondarenko, Y., Van Baalen, M., and Blankevoort, T. A white paper on neural network quantization. *arXiv preprint arXiv:2106.08295*, 2021.
- Nagel, M., Fournarakis, M., Bondarenko, Y., and Blankevoort, T. Overcoming oscillations in quantization-aware training. In *ICML*, pp. 16318–16330, 2022.
- Nie, S., Zhu, F., You, Z., Zhang, X., Ou, J., Hu, J., Zhou, J., Lin, Y., Wen, J.-R., and Li, C. Large language diffusion models. *arXiv preprint arXiv:2502.09992*, 2025.
- Penrose, R. A generalized inverse for matrices. In *Mathematical Proceedings of the Cambridge Philosophical Society*, pp. 406–413, 1955.
- Sapkota, R., Qureshi, R., Hadi, M. U., Hassan, S. Z., Sadak, F., Shoman, M., Sajjad, M., Dharejo, F. A., Paudel, A., Li, J., et al. Multi-modal llms in agriculture: A comprehensive review. *IEEE Transactions on Automation Science and Engineering*, 2025.

- Shao, W., Chen, M., Zhang, Z., Xu, P., Zhao, L., Li, Z., Zhang, K., Gao, P., Qiao, Y., and Luo, P. Omniquant: Omnidirectionally calibrated quantization for large language models. *arXiv preprint arXiv:2308.13137*, 2023.
- Sun, Y., Liu, R., Bai, H., Bao, H., Zhao, K., Li, Y., Hu, J., Yu, X., Hou, L., Yuan, C., et al. Flatquant: Flatness matters for llm quantization. *ICML*, 2025.
- Team, G., Anil, R., Borgeaud, S., Alayrac, J.-B., Yu, J., Soricut, R., Schalkwyk, J., Dai, A. M., Hauth, A., Millican, K., et al. Gemini: a family of highly capable multimodal models. *arXiv preprint arXiv:2312.11805*, 2023.
- Thirunavukarasu, A. J., Ting, D. S. J., Elangovan, K., Gutierrez, L., Tan, T. F., and Ting, D. S. W. Large language models in medicine. *Nature Medicine*, 29(8):1930–1940, 2023.
- Tian, Y., Liang, Y., Sun, J., Zhang, S., Yang, G., Shu, Y., Fang, S., Guo, T., Han, K., Xu, C., et al. From next-token to next-block: A principled adaptation path for diffusion llms. *arXiv preprint arXiv:2512.06776*, 2025.
- Touvron, H., Lavril, T., Izacard, G., Martinet, X., Lachaux, M.-A., Lacroix, T., Rozière, B., Goyal, N., Hambro, E., Azhar, F., et al. Llama: Open and efficient foundation language models. *arXiv preprint arXiv:2302.13971*, 2023.
- Tseng, A., Chee, J., Sun, Q., Kuleshov, V., and De Sa, C. Quip#: Even better llm quantization with hadamard incoherence and lattice codebooks. *ICML*, 2024.
- Wang, X., Song, D., Chen, S., Zhang, C., and Wang, B. Longllava: Scaling multi-modal llms to 1000 images efficiently via a hybrid architecture. *arXiv preprint arXiv:2409.02889*, 2024.
- Wang, X., Xu, C., Jin, Y., Jin, J., Zhang, H., and Deng, Z. Diffusion llms can do faster-than-ar inference via discrete diffusion forcing. *arXiv preprint arXiv:2508.09192*, 2025.
- Wu, C., Zhang, H., Xue, S., Diao, S., Fu, Y., Liu, Z., Molchanov, P., Luo, P., Han, S., and Xie, E. Fastd1lm v2: Efficient block-diffusion llm. *arXiv preprint arXiv:2509.26328*, 2025.
- Wu, S., Fei, H., Qu, L., Ji, W., and Chua, T.-S. Next-gpt: Any-to-any multimodal llm. In *ICML*, 2024.
- Xia, Y., Fu, F., Zhang, W., Jiang, J., and Cui, B. Efficient multi-task llm quantization and serving for multiple lora adapters. In *NeurIPS*, pp. 63686–63714, 2024.
- Xiao, B., Xia, B., Yang, B., Gao, B., Shen, B., Zhang, C., He, C., Lou, C., Luo, F., Wang, G., et al. Mimo-v2-flash technical report. *arXiv preprint arXiv:2601.02780*, 2026.
- Xiao, G., Lin, J., Seznec, M., Wu, H., Demouth, J., and Han, S. Smoothquant: Accurate and efficient post-training quantization for large language models. In *ICML*, pp. 38087–38099, 2023.
- Xu, C. and Yang, D. D1lmquant: Quantizing diffusion-based large language models. *arXiv preprint arXiv:2508.14090*, 2025.
- Xu, J., Guo, Z., He, J., Hu, H., He, T., Bai, S., Chen, K., Wang, J., Fan, Y., Dang, K., et al. Qwen2. 5-omni technical report. *arXiv preprint arXiv:2503.20215*, 2025.
- Yang, A., Li, A., Yang, B., Zhang, B., Hui, B., Zheng, B., Yu, B., Gao, C., Huang, C., Lv, C., et al. Qwen3 technical report. *arXiv preprint arXiv:2505.09388*, 2025a.
- Yang, L., Tian, Y., Li, B., Zhang, X., Shen, K., Tong, Y., and Wang, M. Mmada: Multimodal large diffusion language models. *arXiv preprint arXiv:2505.15809*, 2025b.
- Yao, Y., Yu, T., Zhang, A., Wang, C., Cui, J., Zhu, H., Cai, T., Li, H., Zhao, W., He, Z., et al. Minicpm-v: A gpt-4v level mllm on your phone. *arXiv preprint arXiv:2408.01800*, 2024.
- Yao, Z., Li, C., Wu, X., Youn, S., and He, Y. A comprehensive study on post-training quantization for large language models. *arXiv preprint arXiv:2303.08302*, 2023.
- Ye, J., Xie, Z., Zheng, L., Gao, J., Wu, Z., Jiang, X., Li, Z., and Kong, L. Dream 7b: Diffusion large language models. *arXiv preprint arXiv:2508.15487*, 2025.
- Yu, J., Zhou, S., Yang, D., Li, S., Wang, S., Hu, X., Xu, C., Xu, Z., Shu, C., and Yuan, Z. Mquant: Unleashing the inference potential of multimodal large language models via static quantization. In *ACM MM*, pp. 1783–1792, 2025.
- Yue, X., Ni, Y., Zhang, K., Zheng, T., Liu, R., Zhang, G., Stevens, S., Jiang, D., Ren, W., Sun, Y., et al. Mmmu: A massive multi-discipline multimodal understanding and reasoning benchmark for expert agi. In *CVPR*, pp. 9556–9567, 2024.
- Zhang, A., Wang, N., Deng, Y., Li, X., Yang, Z., and Yin, P. Magr: Weight magnitude reduction for enhancing post-training quantization. In *NeurIPS*, pp. 85109–85130, 2024.
- Zhang, D., Wang, G., Xue, J., Fang, K., Zhao, L., Ma, R., Ren, S., Liu, S., Guo, T., Zhuang, W., et al. Mimo-audio: Audio language models are few-shot learners. *arXiv preprint arXiv:2512.23808*, 2025a.
- Zhang, T., Li, Z., Yan, X., Qin, H., Guo, Y., and Zhang, Y. Quant-d1lm: Post-training extreme low-bit quantization for diffusion large language models. *arXiv preprint arXiv:2510.03274*, 2025b.

Zhao, W. X., Zhou, K., Li, J., Tang, T., Wang, X., Hou, Y., Min, Y., Zhang, B., Zhang, J., Dong, Z., et al. A survey of large language models. *arXiv preprint arXiv:2303.18223*, 2023.

Zhou, Z., Ning, X., Hong, K., Fu, T., Xu, J., Li, S., Lou, Y., Wang, L., Yuan, Z., Li, X., et al. A survey on efficient inference for large language models. *arXiv preprint arXiv:2404.14294*, 2024.

Zhu, D., Chen, J., Shen, X., Li, X., and Elhoseiny, M. Minigt-4: Enhancing vision-language understanding with advanced large language models. *arXiv preprint arXiv:2304.10592*, 2023.

Appendix

Contents

A	Theoretical Analysis	14
A.1	Proof of Proposition 1	14
A.2	Proof of Theorem 2	14
B	Related Work	15
B.1	Multimodal and Diffusion LLMs	15
B.2	Quantization for LLMs	15
C	Implementation Details	16
C.1	Calibration Datasets	16
C.2	Evaluation Benchmarks	16
C.3	Base Models	17
C.4	Baselines	17
C.5	Implementation Recipe	17
C.6	Hyperparameter Settings	18
C.7	Detailed Algorithm Flow	18
D	Additional Results	18
D.1	Activation Visualization	18
D.2	Case Studies	18
E	Reproducibility	19
F	Limitations	19
G	Use of LLMs in Writing	20

A. Theoretical Analysis

A.1. Proof of Proposition 1

Recall. To satisfy $XP\tilde{P}W^\top = XW^\top$, the product $P\tilde{P}$ belongs to the set

$$\left\{ Z - P_X(Z - I)P_W \mid Z \in \mathbb{R}^{d \times d} \right\} \supseteq \{I\},$$

which strictly contains the singleton $\{I\}$. Consequently, the constraint admits a solution space that is strictly larger than the set of exact inverses (for which $P\tilde{P} = I$).

Proof.

$$XP\tilde{P}W^\top = XW^\top \implies XP\tilde{P}W^\top - XW^\top = 0 \quad (11)$$

$$X(P\tilde{P} - I)W^\top = 0 \quad (12)$$

According to the general solution for $AXB = C$, see Lemma 1, we have:

$$X(P\tilde{P} - I)W^\top = 0 \implies P\tilde{P} - I = Z - A^\dagger AZBB^\dagger \quad (13)$$

$$P\tilde{P} = Z - A^\dagger AZBB^\dagger + I \quad (14)$$

$$= Z - A^\dagger A(Z - I)BB^\dagger \quad (Z := Z - I) \quad (15)$$

□

Lemma 1 (Solving $AXB = C$ (Penrose, 1955)). A necessary and sufficient condition for the equation $AXB = C$ to have a solution is $AA^\dagger CB^\dagger B = C$, in which case the general solution is

$$X = A^\dagger CB^\dagger + Z - A^\dagger AZBB^\dagger, \quad (16)$$

where Z is arbitrary.

Proof.

$$AXB = C \implies C = AXB = AA^\dagger AXBB^\dagger B = A(A^\dagger CB^\dagger)B. \quad (17)$$

$A^\dagger CB^\dagger$ is the particular solution of $AXB = C$. For the general solution, we are solving $AXB = 0$.

$$X = Z - A^\dagger AZBB^\dagger \implies AXB = A(Z - A^\dagger AZBB^\dagger)B \quad (18)$$

$$= AZB - AA^\dagger AZBB^\dagger B \quad (19)$$

$$= AZB - AZB = 0 \quad (20)$$

If X is one solution of $AXB = 0$, then

$$AXB = 0 \implies X = X - 0 = X - A^\dagger(AXB)B^\dagger \quad (21)$$

□

A.2. Proof of Theorem 2

Recall. Given $U, U_X, U_{X'}$ be semi-orthogonal basis matrices forming an orthogonal decomposition of \mathbb{R}^d , such that $XU_{X'} = 0$ and $X'U_X = 0$. If we define the orthogonal matrix $\tilde{P} = [U, U_X, U_{X'}]^\top$ and the masked transformations $P = [U, U_X, 0]$ and $P' = [U, 0, U_{X'}]$, then for any weight matrix W , the equalities

$$XP\tilde{P}W^\top = XW^\top \quad \text{and} \quad X'P'\tilde{P}W^\top = X'W^\top$$

hold.

Proof. Give the identity property of the orthogonal matrix \tilde{P} , we have:

$$\tilde{P}\tilde{P}^\top = [U, U_X, U_{X'}] \begin{bmatrix} U^\top \\ U_X^\top \\ U_{X'}^\top \end{bmatrix} \quad (22)$$

$$= UU^\top + U_X U_X^\top + U_{X'} U_{X'}^\top \quad (23)$$

$$= I_d \quad (24)$$

Since the rank-deficiency of X , we have $\text{rank}(X) = r + r_1 < d$. We can find a matrix $U_{X'} \in \mathbb{R}^{d \times r_2}$, $r_2 = d - (r + r_1)$ satisfy $XU_{X'}U_{X'}^\top = 0$, where $U_{X'}U_{X'}^\top$ projects X to the its kernel space. Therefore,

$$XP\tilde{P}W^\top = X[U, U_X, 0] \begin{bmatrix} U^\top \\ U_X^\top \\ U_{X'}^\top \end{bmatrix} W^\top \quad (25)$$

$$= X(UU^\top + U_X U_X^\top)W^\top \quad (26)$$

$$= X(I_d - U_{X'}U_{X'}^\top)W^\top \quad (\tilde{P}\tilde{P}^\top = I_d) \quad (27)$$

$$= XW^\top - \underbrace{XU_{X'}U_{X'}^\top}_{0}W^\top = XW^\top \quad (28)$$

This also holds for mX' , for its rank-deficiency $\text{rank}(X') = r + r_2 < d$. Therefore:

$$X'P'\tilde{P}W^\top = X'(I_d - U_X U_X^\top)W^\top = X'W^\top - X'U_X U_X^\top W^\top = X'W^\top. \quad (29)$$

□

B. Related Work

B.1. Multimodal and Diffusion LLMs

Large Language Models (LLMs) (Achiam et al., 2023; Touvron et al., 2023; Thirunavukarasu et al., 2023; Zhao et al., 2023; Chang et al., 2024; Kaddour et al., 2023) have demonstrated remarkable success in generating textual tokens, paving the way for advanced extensions such as Multimodal LLMs (MLLMs) (Team et al., 2023; Luo et al., 2025; Xiao et al., 2026; Zhang et al., 2025a; Sapkota et al., 2025; Lyu et al., 2023; Wang et al., 2024), which integrate modalities like vision, and diffusion LLMs (dLLMs) (Nie et al., 2025; Ye et al., 2025; Wu et al., 2025; Jin et al., 2025; Tian et al., 2025), which introduce a denoising mechanism on masked tokens to enable simultaneous multi-token prediction. Typically, MLLMs incorporate a visual encoder to process visual inputs, followed by a projector to align different modalities with a powerful decoder-based LLM. Since the release of ChatGPT, researchers augment open-source LLMs (e.g., the LLaMA series (Touvron et al., 2023)) with visual perception capabilities, establishing a widely adopted paradigm exemplified by MiniGPT-4 (Zhu et al., 2023) and NExT-GPT (Wu et al., 2024). Subsequent research has scaled data and parameters, leading to the release of Qwen-VL (Bai et al., 2025), InternVL (Chen et al., 2024), and MiniCPM-V (Yao et al., 2024). Most recent works propose a unified multimodal paradigm that eliminates the separate vision projector, opting instead for a tightly coupled visual-text architecture capable of both understanding and generation. Meanwhile, dLLMs explore the prediction of multiple masked tokens, inspired by prior discrete diffusion modeling with absorbing states (Nie et al., 2025). LLaDA (Nie et al., 2025) and Dream (Ye et al., 2025) successfully implement this diffusion process in billion-parameter models, achieving performance comparable to purely autoregressive LLMs. In this paper, we target these two advanced paradigms and formulate a unified quantization framework for both.

B.2. Quantization for LLMs

Quantization significantly improves efficiency by reducing the precision, particularly for LLMs. Quantization-Aware Training (QAT) adopts low-bit precision directly during training (Nagel et al., 2022; Chen et al., 2025; Liu et al., 2024c; Bondarenko et al., 2024; Du et al., 2024), whereas Post-Training Quantization (PTQ) is applied to pre-trained models, aiming to retain their original capabilities in a resource-efficient manner (Yao et al., 2023). Within the PTQ paradigm,

recent research is generally categorized into weight-only (Frantar et al., 2022; Lin et al., 2024b) and weight-activation quantization (Tseng et al., 2024; Ashkboos et al., 2024; Lin et al., 2024a), where the latter further quantizes activations to achieve higher efficiency but presents greater challenges. Several works (Shao et al., 2023; Bhalgat et al., 2020) focus on managing clip thresholds and fine-grained scales to constrain value ranges. In contrast, SmoothQuant (Xiao et al., 2023) migrates the difficulty of quantization from activations to weights using a diagonal matrix, while QuaRot (Ashkboos et al., 2024) introduces the Hadamard transformation to mitigate outliers, establishing a one-to-one transformation that ensures mathematical equivalence. Recent studies extend this transformation-based paradigm by making these matrices learnable (Lin et al., 2024a; Hu et al., 2025) and more flexible, evolving from simple rotations (Liu et al., 2024d) to general affine transformations (Ma et al., 2024). Notably, FlatQuant (Sun et al., 2025) incorporates the Kronecker product with affine transformations, achieving state-of-the-art quantization quality on LLMs. Researchers have also specialized these techniques for dLLMs (Xu & Yang, 2025; Lin et al., 2025a; Zhang et al., 2025b) and MLLMs (Yu et al., 2025), which involve different token types. However, these efforts mainly focus on optimizing scales and calibrating the dataset, setting transformation advancement aside. In this paper, we pioneer the exploration of flexible transformations beyond one-to-one for LLMs, specifically dLLMs and MLLMs, that process diverse input types with distinct activation distributions.

C. Implementation Details

C.1. Calibration Datasets

- **WikiText2** (Merity et al., 2016)⁵ is a language modeling dataset comprising approximately 2 million tokens on Wikipedia. It maintains a vocabulary size of 33,278 words and retains the original document structure, including full punctuation and capitalization. We directly concatenate different sequences and split them into 128 samples with 2048 tokens for quantization calibration of dLLMs.
- **COCO-Cap** (Lin et al., 2014)⁶ is a large-scale multimodal collection consisting of approximately 120,000 images derived from the MS COCO dataset, with each image annotated with five independent human-generated captions. We randomly select 256 samples from its validation split, serving as the calibration dataset for MLLM quantization.

C.2. Evaluation Benchmarks

- **GSM8K** (Cobbe et al., 2021) is a dataset of approximately 8,500 high-quality, linguistically diverse grade school math word problems created by human writers. We employ its test split, which contains 1,319 examples in total.
- **Human-Eval** (Chen, 2021) is a code generation benchmark released by OpenAI, consisting of 164 hand-written programming problems in Python. Each problem includes a function signature, a docstring, and a set of hidden unit tests.
- **Math500** (Hendrycks et al., 2021) is a curated subset of the larger MATH dataset, containing 500 challenging mathematics problems covering diverse subjects such as algebra, geometry, and calculus. It serves as a robust benchmark for evaluating the advanced mathematical problem-solving capabilities of LLMs.
- **MMMU** (Yue et al., 2024) is a large-scale benchmark designed to evaluate expert-level multimodal reasoning. It comprises approximately 11,500 questions derived from college exams, quizzes, and textbooks across six core disciplines and 30 distinct subjects. We use its validation split, comprising 900 multiple-choice questions.
- **MMBench** (Liu et al., 2024b) is a comprehensive evaluation pipeline designed to assess the fine-grained perception and reasoning abilities of MLLMs. It employs a circular evaluation strategy with multiple-choice questions to ensure robust performance assessment across various perceptual and cognitive dimensions.
- **RealworldQA** is a benchmark designed to test spatial and physical reasoning in real-world scenarios. It features high-quality images taken from vehicles and egocentric views, challenging models to answer questions about object relations and environmental context in unconstrained, realistic settings.

⁵<https://huggingface.co/datasets/Salesforce/wikitext>

⁶<https://huggingface.co/datasets/lmms-lab/COCO-Caption>

The evaluation of dLLMs is evaluated by `LM_Eval`⁷ and further accelerated with `Fast-dLLM`⁸. The evaluation of MLLMs is evaluated by `lmms-eval`⁹.

C.3. Base Models

- **LLaDA** (Nie et al., 2025) is a generative Large Language Model built on a diffusion architecture by employing a masked diffusion strategy. It iteratively denoises the entire sequence in parallel during both training and inference, demonstrating that diffusion models can achieve generation quality and in-context learning capabilities comparable to autoregressive baselines. We use its instruction version, `LLaDA-8B-Instruct`, for our evaluation.
- **Dream** (Ye et al., 2025) is a diffusion large language model that employs discrete diffusion modeling to optimize the sequences in parallel. Dream is initialized with weights from `Qwen2.5 7B` and is continually pre-trained to adapt the diffusion architecture. We use its instruction version, `Dream-v0-Instruct-7B`, for our evaluation.
- **QwenVL** (Bai et al., 2025) is a vision-language model built upon the Qwen foundation, designed to handle high-resolution image inputs and fine-grained visual grounding tasks. It incorporates position-aware visual adapters that allow it to perform complex tasks, establishing itself as a robust open-source benchmark for general-purpose multimodal perception and interaction. We use `Qwen2.5-VL-7B-Instruct` for our evaluation.
- **InternVL** (Chen et al., 2024) employs a progressive scaling strategy that aligns a 6B vision encoder with smaller LLMs before seamlessly transferring weights to larger models to cut computational costs. The well-designed data pipelines and the advanced reweighting technique that balance gradients across diverse response lengths and enhance the visual understanding. Here we use `InternVL2.5-8B` for our evaluation.

C.4. Baselines

- **RTN** is the straightforward quantization strategy that maps floating-point values to the nearest integer representation without additional optimization or calibration.
- **SmoothQuant** (Xiao et al., 2023) uses a diagonal scales to smooth activation outliers by migrating the quantization difficulty from activations to weights.
- **QuaRot** (Ashkboos et al., 2024) uses randomized Hadamard transforms to rotate weights and activations into a space where outliers are suppressed, enabling outlier-free 4-bit quantization.
- **FlatQuant** (Sun et al., 2025) is designed to improve low-bit quantization by flattening the activation distributions using similar rotation techniques, specifically optimized for efficient deployment on hardware.

C.5. Implementation Recipe

In the following, we first review the one-to-one transformation recipe, exemplified by FlatQuant. Then we provide a comprehensive implementation of FreeAct.

One-to-one recipe. Give a linear layer equipped with weight $\mathbf{W} \in \mathbb{R}^{d' \times d}$, the input activation is denoted as $\mathbf{X} \in \mathbb{R}^{n \times d}$, satisfying $\mathbf{Y} = \mathbf{X}\mathbf{W}^\top \in \mathbb{R}^{n \times d'}$. For the weight side, $\widetilde{\mathbf{W}} \leftarrow \mathbf{P}_l^{-1} \times \widetilde{\mathbf{W}} / \text{diag}(\mathbf{c}) \times (\mathbf{P}_r^{-1})^\top$. And $\mathbf{P}_l := \mathbf{U}_l \times \text{diag}(\mathbf{s}_l) \times \mathbf{V}_l^\top$ is constructed via SVD to guarantee the invertibility of \mathbf{P} . \mathbf{U} and \mathbf{V} are both orthogonal matrices, and \mathbf{s} is the vector containing singular values. The transformed weight $\widetilde{\mathbf{W}}$ is then clipped, operating $\text{clamp}(\widetilde{\mathbf{W}}, s_{\widetilde{\mathbf{W}}}^{\min}, s_{\widetilde{\mathbf{W}}}^{\max})$, where $s_{\widetilde{\mathbf{W}}}^{\min} := (\min \widetilde{\mathbf{W}}) \cdot \sigma(\alpha_{\widetilde{\mathbf{W}}}^{\min})$ and $s_{\widetilde{\mathbf{W}}}^{\max} := (\max \widetilde{\mathbf{W}}) \cdot \sigma(\alpha_{\widetilde{\mathbf{W}}}^{\max})$. α is the learnable clip threshold. For the activation side, similarly, $\widetilde{\mathbf{X}} \leftarrow \mathbf{P}_l^\top \times \mathbf{X} \cdot \text{diag}(\mathbf{c}) \times \mathbf{P}_r$, followed by $\text{clamp}(\widetilde{\mathbf{X}}, s_{\widetilde{\mathbf{X}}}^{\min}, s_{\widetilde{\mathbf{X}}}^{\max})$. After the transformation, we adopt the quantizer from GPTQ. Specifically, the quantization scale for weight is estimated by the minimum and maximum values per channel without MSE search. For the activation, the scale is estimated per token.

⁷<https://github.com/EleutherAI/lm-evaluation-harness>

⁸<https://github.com/NVlabs/Fast-dLLM>

⁹<https://github.com/EvolvingLLMs-Lab/lmms-eval>

Equivalence. The equivalence of one-to-one transformation methods can be simply verified by the following equations: $\widetilde{\mathbf{X}}\widetilde{\mathbf{W}}^\top = (\mathbf{P}_l^\top \times \mathbf{X} \cdot \text{diag}(\mathbf{c}) \times \mathbf{P}_r)(\mathbf{P}_l^{-1} \times \mathbf{W}/\text{diag}(\mathbf{c}) \times (\mathbf{P}_r^{-1})^\top)^\top = \mathbf{X}\mathbf{P} \times \mathbf{P}^{-1}\mathbf{W}^\top = \mathbf{X}\mathbf{W}^\top$.

More-to-one recipe (FreeAct). The processing for one linear layer mostly follows the one-to-one recipe. Let $\mathbf{X} := \mathbf{X} \cdot \text{diag}(\mathbf{c})$ and $\mathbf{W} := \mathbf{W}/\text{diag}(\mathbf{c})$, we assign the same projection matrix for different activations, *i.e.*, \mathbf{X} and \mathbf{X}' , yet masking its different portions. For instance, $\widetilde{\mathbf{X}} := (\mathbf{P}_l^\top \times \mathbf{X} \cdot \text{diag}(\mathbf{c}) \times \mathbf{P}_r) \odot \mathbf{m}$, where $\mathbf{m} \in \{0, 1\}^d$ is a binary vector and \odot represents the element wise multiplication. \mathbf{m} controls the utilization of different components for different activation types. For other parts, we keep the same as the one-to-one recipe. The *equivalence* of the more-to-one recipe is proved in Appendix A.2.

Implementation for dLLMs. We utilize the LLaDA and Dream implementations from Fast-dLLM to facilitate inference via its optimized caching techniques. The maximum number of generated tokens is set to 256 using 8 time blocks. For calibration, we construct 128 examples containing 2,048 text tokens followed by 256 mask tokens. The activation indices are determined by the [MASK] token ID prior to the next denoising step; consequently, we do not need to explicitly simulate distinct diffusion steps. To accelerate the calibration process, we save all input and output hidden states per layer and train these layers in parallel.

Implementation for MLLMs. We adopt tailored strategies for the various components within the MLLMs. For the LM backbone, we employ FreeAct as it effectively handles diverse activation inputs, such as vision and text. Given that the sequence length for each calibration example is relatively short, we use 256 examples for the calibration process. Activation indices are determined by the [IMG] token ID during prefilling. We apply FlatQuant to the vision model due to its homogeneous tokens and adopt RTN for the MLP projector. Similar to the dLLM setup, we save all input and output hidden states for both the vision encoder and LM decoder to facilitate parallelized training and faster calibration.

C.6. Hyperparameter Settings

We employ the AdamW optimizer (Loshchilov & Hutter, 2017) to optimize the quantization parameters, including the transformation matrices and the clip threshold, while freezing the model parameters. We set the learning rate as 1×10^{-3} and train the parameters on calibrated datasets for 15 epochs. The number of samples is 128 for dLLMs and 256 for MLLMs. The transformation matrix is initialized as a random orthogonal matrix and is restricted to being orthogonal during the optimization. The clip threshold is initialized as 4.0. We keep these hyperparameters the same for both baselines and FreeAct. The key hyperparameters for FreeAct are $\{r, r_1, r_2\}$. To simplify the implementation, we set $r_1 = r_2 = d/k$. We set $k = 32$ by default.

C.7. Detailed Algorithm Flow

In this section, we provide the training algorithm flow of FreeAct in Algorithm 1.

D. Additional Results

In this section, we provide the full illustrations of activations per layer across different models.

D.1. Activation Visualization

We provide the full details of activation distributions for all layers across four evaluated models, as shown in Figures 11, 12, 13, and 14. We also provide the full quantization errors across four models in Figures 9 and 10.

D.2. Case Studies

In this section, we provide the cases generated by different models to demonstrate the effectiveness of FreeAct (see Figures 15, 16, 17, and 18).

Algorithm 1 FreeAct Algorithm Flow

Require: Calibration dataset $\mathcal{D} = \{\mathbf{X}_k\}_{k=1}^N$ where $\mathbf{X}_k \in \mathbb{R}^{L \times d}$, pre-trained weights $\mathbf{W} \in \mathbb{R}^{d \times d_{out}}$, r, r_1, r_2 .

Ensure:

- 1: Optimized orthogonal matrix $\tilde{\mathbf{P}} \in \mathbb{R}^{d \times d}$. Other quantization parameters (scales, clip threshold).
- 2: **Initialization:**
- 3: Initialize $\tilde{\mathbf{P}} \in d \times d$ as a random orthogonal matrix.
- 4: **while** not converged **do**
- 5: **for** each batch of input activations $\hat{\mathbf{X}} \in \mathbb{R}^{B \times L \times d}$ in \mathcal{D} **do**
- 6: ① **Token Indexing.**
 Identify indices based on token types (e.g., Vision/Text or Unmasked/Masked):
 $\mathcal{G} := \{i \mid \mathcal{I}(\hat{\mathbf{X}}_{:,i,:}) \text{ is Type A}\}$ $\mathcal{G}' := \{i \mid \mathcal{I}(\hat{\mathbf{X}}_{:,i,:}) \text{ is Type B}\}$
- 7: ② **Dynamic Allocation.**
 $\tilde{\mathbf{P}} \leftarrow [\mathbf{U}, \mathbf{U}_{\mathbf{X}}, \mathbf{U}_{\mathbf{X}'}]^\top \triangleright \mathbf{U} \in \mathbb{R}^{d \times r} \quad \mathbf{U}_{\mathbf{X}} \in \mathbb{R}^{d \times r_1} \quad \mathbf{U}_{\mathbf{X}'} \in \mathbb{R}^{d \times r_2}$
 $\mathbf{P} \leftarrow [\mathbf{U}, \mathbf{U}_{\mathbf{X}}, \mathbf{0}] \in \mathbb{R}^{d \times d}$, where $\mathbf{0} \in \mathbb{R}^{d \times r_2}$
 $\mathbf{P}' \leftarrow [\mathbf{U}, \mathbf{0}, \mathbf{U}_{\mathbf{X}'}] \in \mathbb{R}^{d \times d}$, where $\mathbf{0} \in \mathbb{R}^{d \times r_1}$
- 8: ③ **Grouping**
 $\mathbf{X} \leftarrow \hat{\mathbf{X}}_{:, \mathcal{G}, :} \in \mathbb{R}^{B \times |\mathcal{G}| \times d}$
 $\mathbf{X}' \leftarrow \hat{\mathbf{X}}_{:, \mathcal{G}', :} \in \mathbb{R}^{B \times |\mathcal{G}'| \times d}$
- 9: ④ **Transformation & Quantization**
 $\tilde{\mathbf{W}} \leftarrow \tilde{\mathbf{P}}\mathbf{W} \quad \tilde{\mathbf{X}} \leftarrow \mathbf{X}\mathbf{P}' \quad \tilde{\mathbf{X}}' \leftarrow \mathbf{X}'\mathbf{P}'$
 $\mathbf{Y}_q \leftarrow \mathcal{Q}(\tilde{\mathbf{X}})\mathcal{Q}(\tilde{\mathbf{W}}) \quad \mathbf{Y}'_q \leftarrow \mathcal{Q}(\tilde{\mathbf{X}}')\mathcal{Q}(\tilde{\mathbf{W}})$
- 10: ⑤ **Optimization**
 $\mathcal{L} \leftarrow \|\mathbf{X}\mathbf{W} - \mathbf{Y}_q\|_2^2 + \|\mathbf{X}'\mathbf{W} - \mathbf{Y}'_q\|_2^2$ (Eq. (10))
 Update $\tilde{\mathbf{P}}$ and quantization params to minimize \mathcal{L} .
- 11: **end for**
- 12: **end while**

E. Reproducibility

We provide implementation details, involving illustrative algorithm descriptions in Appendix C and pseudo-code in Section 3.2. The source code will be publicly released for reproducibility.

F. Limitations

We demonstrate the effectiveness of FreeAct through rigorous empirical validation and theoretical support, establishing its conceptual advancement in the field of quantization. Despite these strengths, several limitations remain for future exploration.

1) The current version of FreeAct cannot accept more modalities or diverse input types ($\# > 2$). It can be extended to more complex scenarios, but requires an in-depth investigation into activation distributions. 2) Due to the resource constraints, we

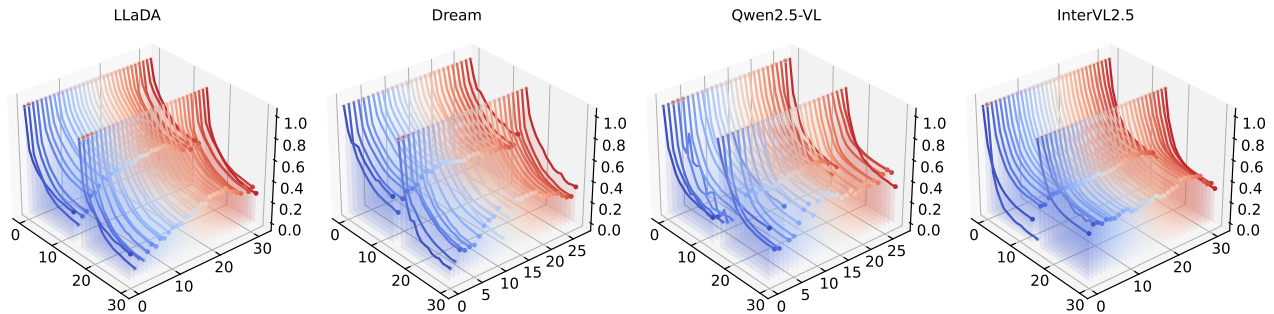


Figure 9. The full losses trained on the calibration dataset for four models. The quantization errors are measured per layer and grouped in terms of different activation types. To better show the differences, the numerical values are normalized.

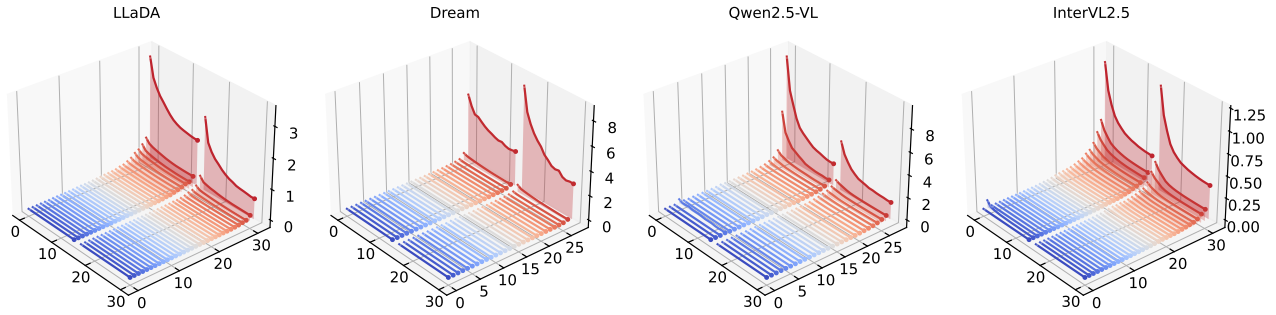


Figure 10. The full losses trained on the calibration dataset for four models. The quantization errors are measured per layer and grouped in terms of different activation types.

do not scale the model size. 3) We do not deploy FreeAct offline while evaluating its effectiveness with fake quantization.

G. Use of LLMs in Writing

We used an LLM solely to polish the writing and correct grammatical issues during the preparation of this submission. The LLM was not involved in any idea generation, experiment design, or analysis. All scientific contributions are entirely made by the authors.

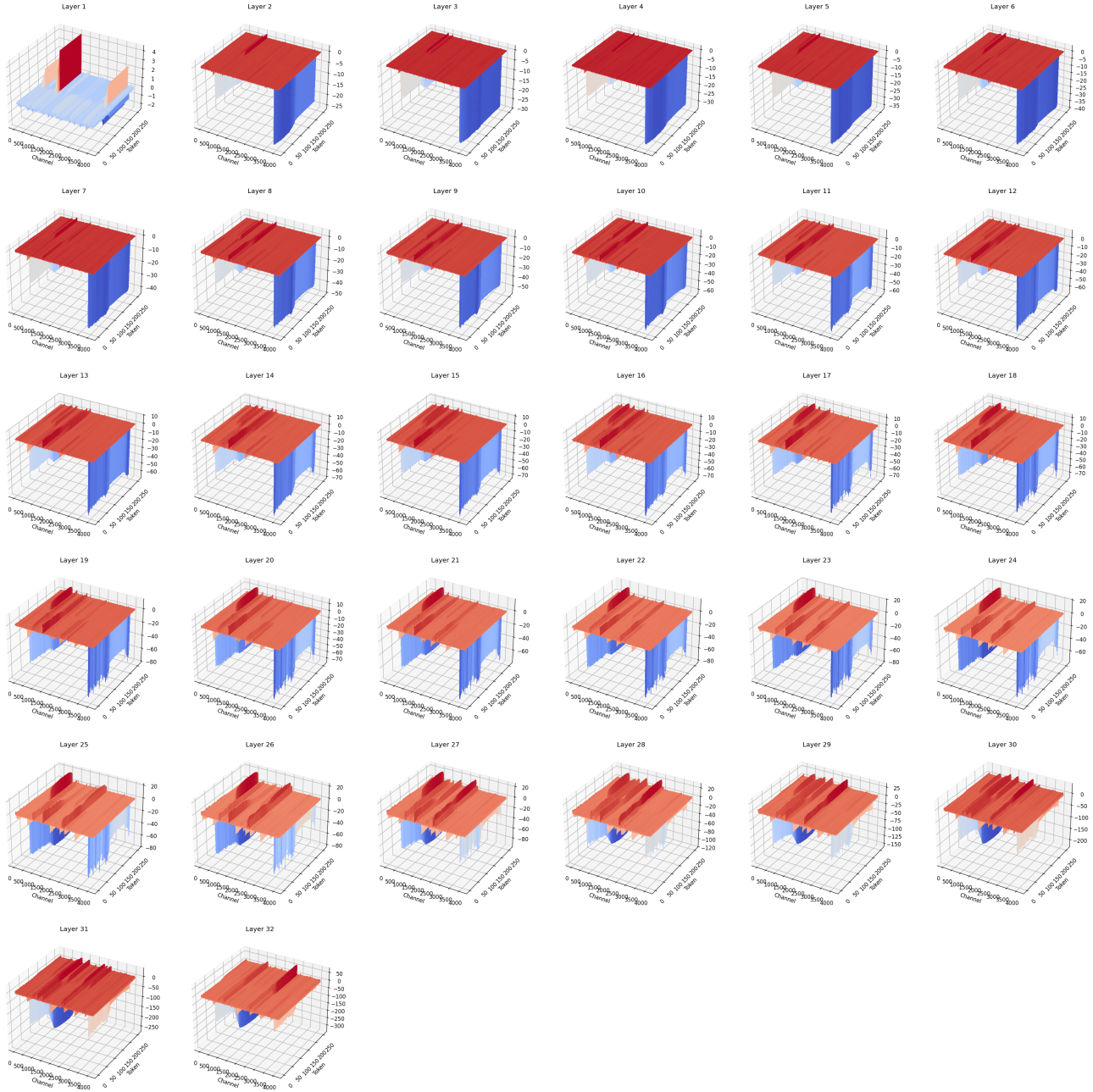


Figure 11. Illustrative examples of activation distributions across different layers on *LLaDA-8B-Instruct*. There is a clear dividing line between unmasked and masked tokens.

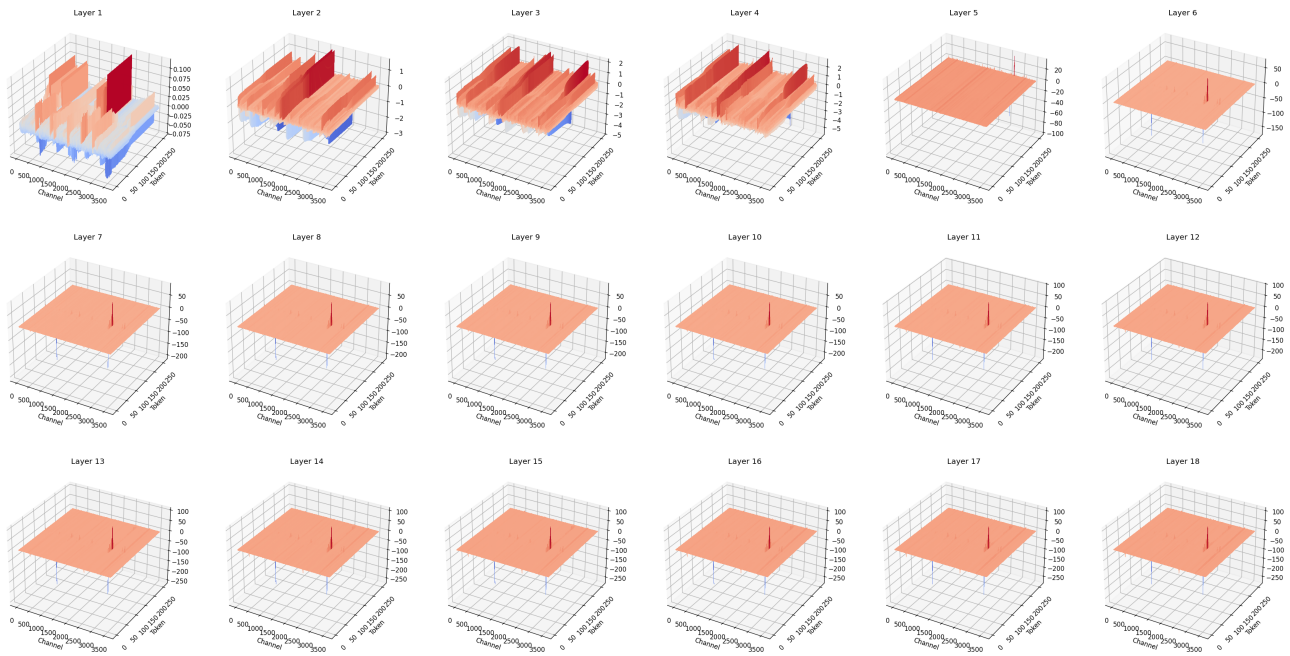


Figure 12. Illustrative examples of activation distributions across different layers on *Dream-v0-Instruct-7B*. There is a clear dividing line and spikes to distinguish unmasked and masked tokens.

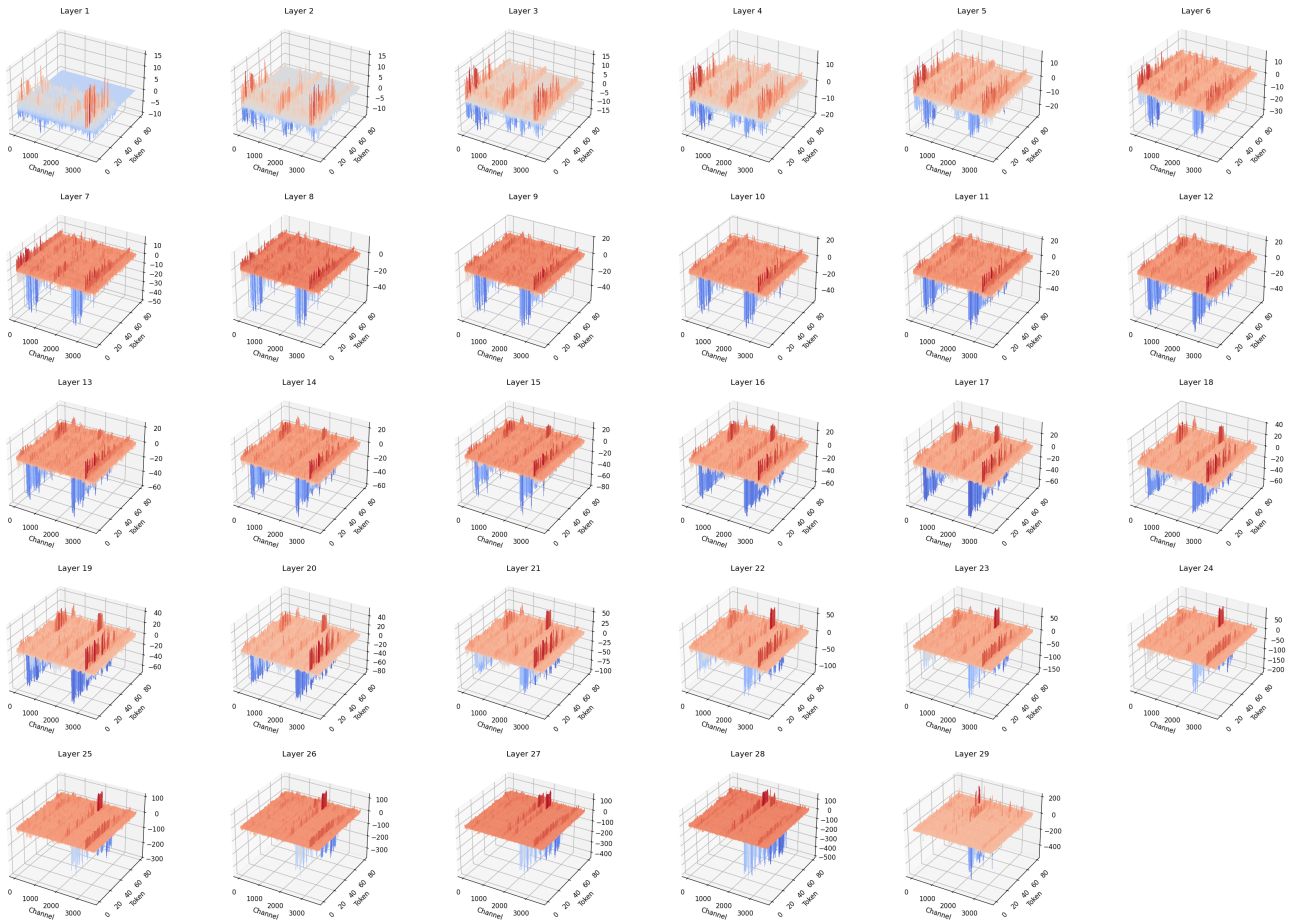


Figure 13. Illustrative examples of activation distributions across different layers on *Qwen2.5-VL-7B-Instruct*. Only the language tower is plotted. There is a clear dividing line to distinguish vision and text tokens.

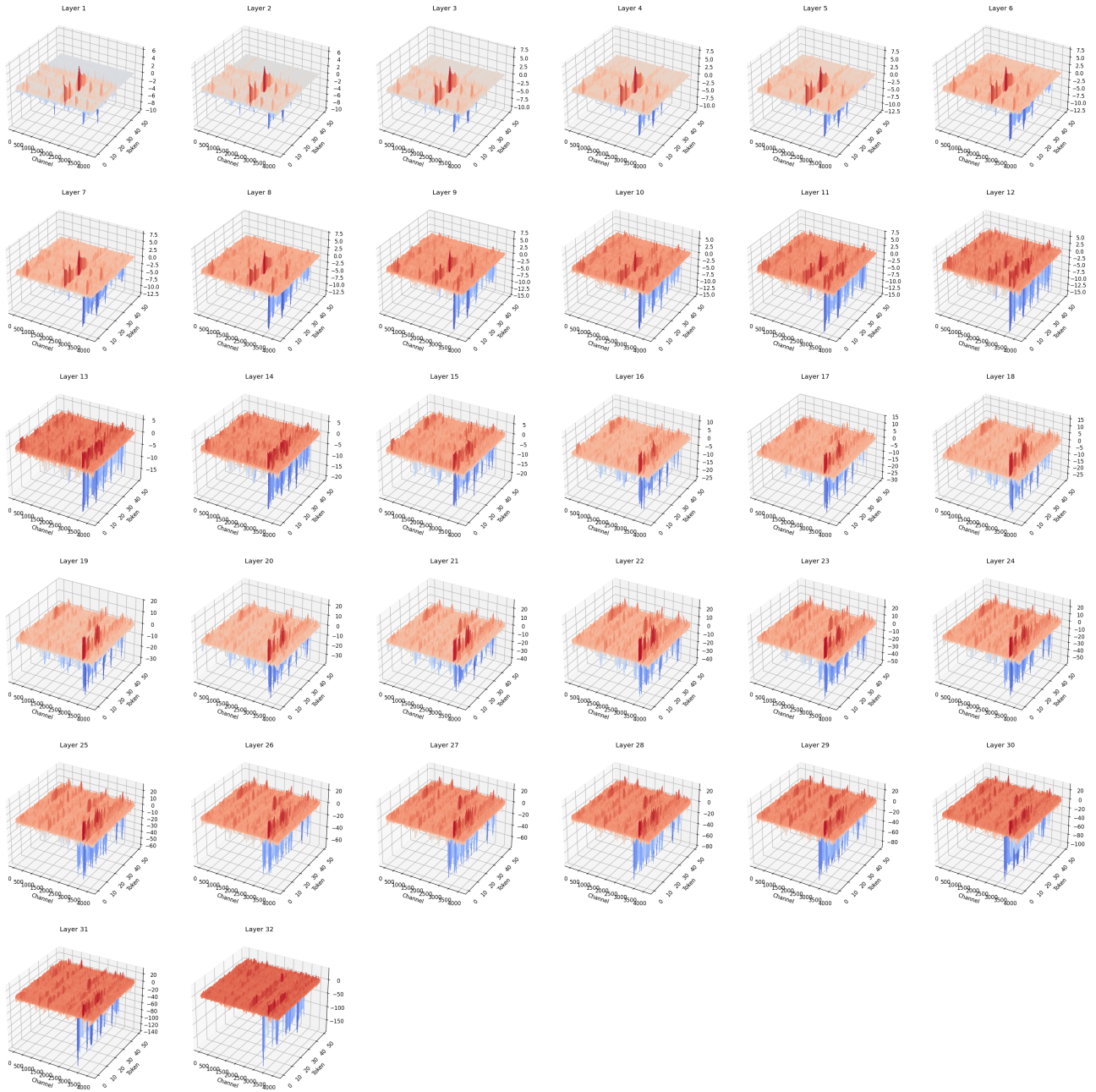


Figure 14. Illustrative examples of activation distributions across different layers on *InternVL2.5-8B*. Only the language tower is plotted. There is a clear dividing line to distinguish vision and text tokens.

Prompt:

<image 1> Baxter Company has a relevant range of production between 15,000 and 30,000 units. The following cost data represents average variable costs per unit for 25,000 units of production. If 30,000 units are produced, what are the per unit manufacturing overhead costs incurred? \nA. \$6\nB. \$7\nC. \$8\nD. \$9\n\nAnswer with the option's letter from the given choices directly.

Response:

BF16 B

RTN (W4A4) Gluten \n\n\n 2 -Pack-gend Stainless (1 Spare Bottle-Pack Clamp
 \n 10-Packerrated Mountedl Movement A S 1/&ombine S1 1 4 Aluminum 0 4 0 0
 Wholesale Decorating Color 2-Packlasses Clamp 1 1S lideh1-Pack Qty5-Pack
 Polymerdden Cabinetslgend-Packreff-Pack -Pack ringe -Pack Bulk Lines2

FreeAct (W4A4) B

Figure 17. Case study of how FreeAct integrates into QWen2.5 VL and performs under the W4A4 quantization setting on the MMMU dataset, compared with the RTN method, which fails to respond.

Prompt:

<image 1> Baxter Company has a relevant range of production between 15,000 and 30,000 units. The following cost data represents average variable costs per unit for 25,000 units of production. If 30,000 units are produced, what are the per unit manufacturing overhead costs incurred? \nA. \$6\nB. \$7\nC. \$8\nD. \$9\n\nAnswer with the option's letter from the given choices directly.

Response:

BF16 B

RTN (W4A4) In n 1, 1 5,000-00 0 s/ 1.5/0. 5/2. The 2010,000 sp?/ 1.5.0 are then
 5/5/10*5 10/0/10/ 5/6?/ \$The The average costs? / 10/6/5.0?. The The ten /5/5 The
 average cost/ 5,000/2/5 The average cost per10? /5%? The average? 5/5 5/0/5?/0

FreeAct (W4A4) B. \$7

Figure 18. Case study of how FreeAct integrates into InternVL2.5 and performs under the W4A4 quantization setting on the MMMU dataset, compared with the RTN method, which fails to respond.